Supporting Information

Photo-induced telomeric DNA damages in human cancer cells

Justin Weynand,[1,2] Harikleia Episkopou,[3] Gabriel Le Berre,[3] Martin Gillard,[1] Jérôme Dejeu,[2] Anabelle Decottignies,*,[3] Eric Defrancq,*,[2] and Benjamin Elias*,[1]

1 Université catholique de Louvain (UCLouvain), Institut de la Matière Condensée et des Nanosciences (IMCN), Molecular Chemistry, Materials and Catalysis (MOST), Place Louis Pasteur 1, bte L4.01.02, B-1348 Louvain-la-Neuve, Belgium

2 Université Grenoble-Alpes (UGA), Département de Chimie Moléculaire, UMR CNRS 5250, CS 40700, 38058 Grenoble, France

3 Université catholique de Louvain (UCLouvain), Genetic and Epigenetic Alterations of Genomes, de Duve Institute, Avenue Hippocrate 75, 1200 Brussels, Belgium

Table of Contents

1. Material and methods

The N^N ligands PIP-$(PEG)_2$-PIP (**7a**) and PIP-$(PEG)_3$-PIP (**7b**), precursor Ru(II) complexes $[Ru(phen)_2Cl_2]$ **8** and $[Ru(TAP)_2Cl_2]$ **9** and complex $[Ru(phen)_2PIP\text{-}(PEG)_3\text{-}PIP(phen)_2Ru]^{4+}$ (**1b**) were synthesized according to described synthetic procedures.[1-4] All solvents and reagents for the synthesis were of reagent grade and were used without any further purification. All solvents for the spectroscopic and electrochemical measurements were of spectroscopic grade. For solubility purposes, all the complexes are converted to the chloride salt for experiments conducted in aqueous media, or to the hexafluorophosphate salt for studies in organic solvents.

2. Synthetic procedures

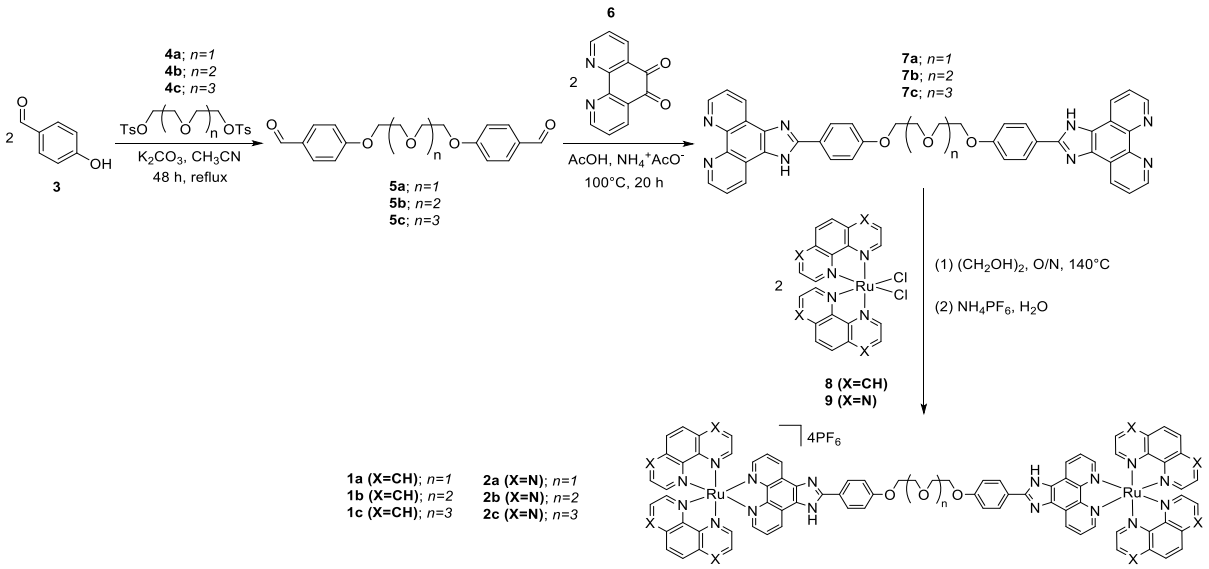

Scheme S1: Synthetic route for the preparation of dinuclear ruthenium(II) complexes **1a-c** and **2a-c**.

PIP-$(PEG)_4$-PIP (**7c**). A solution of 1,10-phenanthroline-5,6-dione **6** (95 mg, 0.45 mmol), dibenzaldehyde **5c** (91 mg, 0.23 mmol), NH_4OAc (180 mg, 2.3 mmol) were dissolved in AcOH (10 mL) and heated at 100°C for 24h. After cooling at RT, the mixture was evaporated under vacuum to afford crude compound. The latter was used in the next step without any further purification.

$[Ru(phen)_2PIP\text{-}(PEG)_2\text{-}PIP(phen)_2Ru].4PF_6$ (**1a**). $[Ru(phen)_2Cl_2]$ (20 mg, 0.037 mmol) and PIP-$(PEG)_2$-PIP **7a** (14 mg, 0.019 mmol) were dissolved in ethylene glycol (5 mL) and heated at 120°C for 20h in the dark and under argon. After cooling and addition of aqueous solution of NH_4PF_6, a precipitate was formed. The latter was washed 3 times with water, EtOH and Et_2O to afford the crude product. Purification by column chromatography on SiO_2 ($CH_3CN/H_2O/KNO_3$(sat) 7/0.5/0.75, v/v/v) gave the final product as a red powder (16 mg, 37%). As the chloride salt was required for the experiments, counter-anion exchange was

achieved upon addition of $tBu_4N^+Cl^-$ to the PF_6^- salt dissolved in acetone. ^1H NMR (500 MHz, CD_3CN): δ (ppm) 9.04 (d, 4H), 8.62-8.59 (m, 8H), 8.30 (d, 4H), 8.27 (s, 8H), 8.11 (bs, 4H), 8.03 (d, 4H), 7.98 (d, 4H), 7.66-7.62 (m, 12H), 7.14 (d, 4H), 4.26 (m, 4H), 3.95 (m, 4H). HRMS Calcd for $C_{90}H_{63}O_3N_{16}Ru_2$ (**1a** - $4PF_6$): 401.83498 Da, found 401.83517 Da.

$[Ru(phen)_2PIP\text{-}(PEG)_4\text{-}PIP(phen)_2Ru].4PF_6$ (**1c**). $[Ru(phen)_2Cl_2]$ (20 mg, 0.037 mmol) and PIP-$(PEG)_4$-PIP **7c** (14 mg, 0.017 mmol) were dissolved in ethylene glycol (5 mL) and heated at 120°C for 20h in the dark and under argon. After cooling and addition of aqueous solution of NH_4PF_6, a solid was formed. The latter was washed 3 times with water, EtOH and Et_2O to afford the crude product. Purification by column chromatography on SiO_2 ($CH_3CN/H_2O/KNO_3$(sat) 7/1/1, v/v/v) gave the final product as a red powder (8 mg, 21%). When the chloride salt was required for the experiments, counter-anion exchange was achieved upon addition of $tBu_4N^+Cl^-$ to the PF_6^- salt dissolved in acetone. ^1H NMR (500 MHz, CD_3CN): δ (ppm) 9.02 (d, 4H), 8.86 (d, 2H), 8.63-8.59 (m, 8H), 8.29-8.24 (m, 12H), 8.09-8.01 (m, 8), 7.95 (m, 4H), 7.14 (m, 4H), 4.21 (m, 4H), 3.84 (m, 4H), 3.67 (m, 4H), 3.63 (m, 4H). HRMS Calcd for $C_{90}H_{70}O_5N_{16}Ru_2$ (**1c** - $4PF_6$): 423.59613 Da, found 423.59713 Da.

$[Ru(TAP)_2PIP\text{-}(PEG)_2\text{-}PIP(TAP)_2Ru].4PF_6$ (**2a**). $[Ru(TAP)_2Cl_2]$ (20 mg, 0.037 mmol) and PIP-$(PEG)_2$-PIP (12 mg, 0.017 mmol) were dissolved in ethylene glycol (5 mL) and heated at 120°C for 20h in the dark and under argon. After cooling and addition of aqueous solution of NH_4PF_6, a solid was formed. The latter was washed 3 times with water, EtOH and Et_2O to afford the crude product. Purification by column chromatography on SiO_2 ($CH_3CN/H_2O/KNO_3$(sat) 7/1/1, v/v/v) gave the final product as a red powder (15 mg, 35%). When the chloride salt was required for the experiments, counter-anion exchange was achieved upon addition of $tBu_4N^+Cl^-$ to the PF_6^- salt dissolved in acetone. ^1H NMR (500 MHz, CD_3CN): δ (ppm) 9.13 (bs, 4H), 8.95 (d, 4H), 8.93 (d, 4H), 8.61 (s, 8H), 8.28 (d, 4H), 8.23 (d, 4H), 8.17 (d, 4H), 8.01 (m, 4H), 7.72 (m, 4H), 7.17 (d, 4H), 4.27 (m, 4H), 3.94 (m, 4H). HRMS Calcd for $C_{82}H_{54}O_3N_{24}Ru_2$ (**2a** - $4PF_6$): 403.57352 Da, found 403.57480 Da.

$[Ru(TAP)_2PIP\text{-}(PEG)_3\text{-}PIP(TAP)_2Ru].4PF_6$ (**2b**). $[Ru(TAP)_2Cl_2]$ (20 mg, 0.037 mmol) and PIP-$(PEG)_3$-PIP (14 mg, 0.0187 mmol) were dissolved in ethylene glycol (5 mL) and heated at 120°C for 20h in the dark and under argon. After cooling and addition of aqueous solution of NH_4PF_6, a solid was formed. The latter was washed 3 times with water, EtOH and Et_2O to afford the crude product. Purification by column chromatography on SiO_2 ($CH_3CN/H_2O/KNO_3$(sat) 7/1/1, v/v/v) gave the final product as a red powder (8.5 mg, 20%). When the chloride salt was required for the experiments, counter-anion exchange was achieved upon addition of $tBu_4N^+Cl^-$ to the PF_6^- salt dissolved in acetone. ^1H NMR (500 MHz, CD_3CN): δ (ppm) 9.12 (m, 4H), 8.95 (d, 4H), 8.91 (d, 4H), 8.60 (s, 8H), 8.25 (m, 8H), 8.18 (d, 4H), 8.00 (d, 4H), 7.69 (m, 4H), 7.08 (m, 4H), 7.17 (d, 4H), 4.18 (m, 4H), 3.83 (m, 4H), 3.69 (m, 4H). HRMS Calcd for $C_{84}H_{58}O_4N_{24}Ru_2$ (**2b** - $4PF_6$): 414.58007 Da, found 414.58049 Da.

$[Ru(TAP)_2PIP\text{-}(PEG)_4\text{-}PIP(TAP)_2Ru].4PF_6$ (**2c**). $[Ru(TAP)_2Cl_2]$ (20 mg, 0.037 mmol) and PIP-$(PEG)_4$-PIP (13 mg, 0.017 mmol) were dissolved in ethylene glycol (5 mL) and heated at 120°C for 20h in the dark and under argon. After cooling and addition of aqueous solution of NH_4PF_6, a solid was formed. The latter was washed 3 times with water, EtOH and Et_2O to afford the crude product. Purification by column chromatography on SiO_2 ($CH_3CN/H_2O/KNO_3$(sat) 7/1/1,

v/v/v) gave the final product as a red powder (7.8 mg, 20%). When the chloride salt was required for the experiments, counter-anion exchange was achieved upon addition of $tBu_4N^+Cl^-$ to the PF_6^- salt dissolved in acetone. ^1H NMR (500 MHz, CD_3CN): δ (ppm) 9.14 (m, 4H), 8.95 (m, 8H), 8.60 (s, 8H), 8.60 (m, 8H), 8.24-8.16 (m, 12H), 8.02 (m, 4H), 7.71 (m, 4H), 7.11 (m, 4H), 4.19 (m, 4H), 3.83 (m, 4H), 3.62-3.64 (m, 8H). HRMS Calcd for $C_{86}H_{62}O_5N_{24}Ru_2$ (**2c** - $4PF_6$): 425.58663 Da, found 425.58760 Da.

3. ^{1}H and 2D NMR spectra of dinuclear Ru(II) complexes

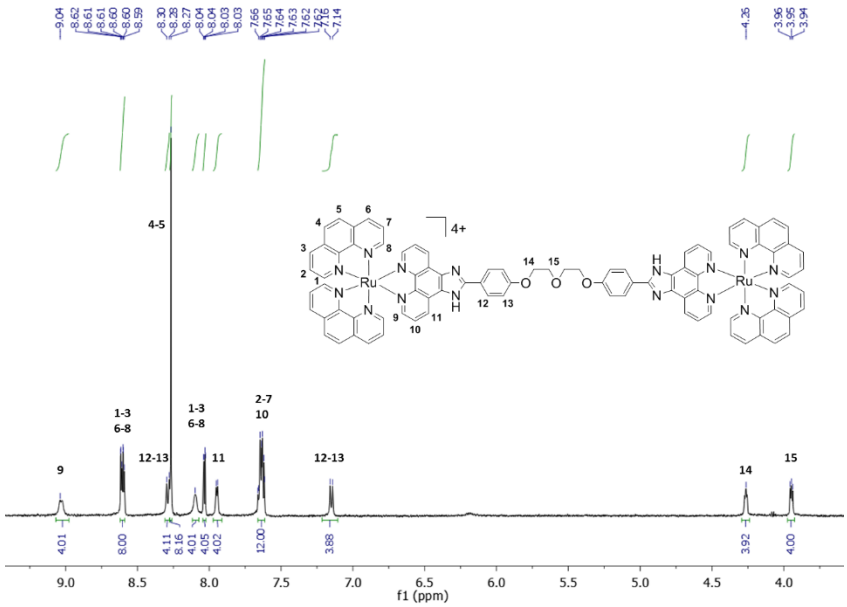

Figure S1: ^{1}H NMR spectra of **1a** (500 MHz, CD_3CN).

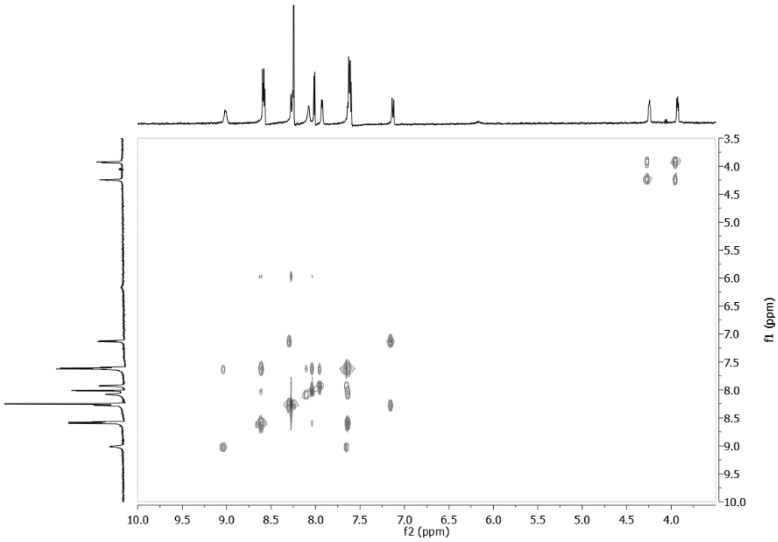

Figure S2: COSY ^{1}H-^{1}H NMR spectra of **1a** (500 MHz, CD_3CN).

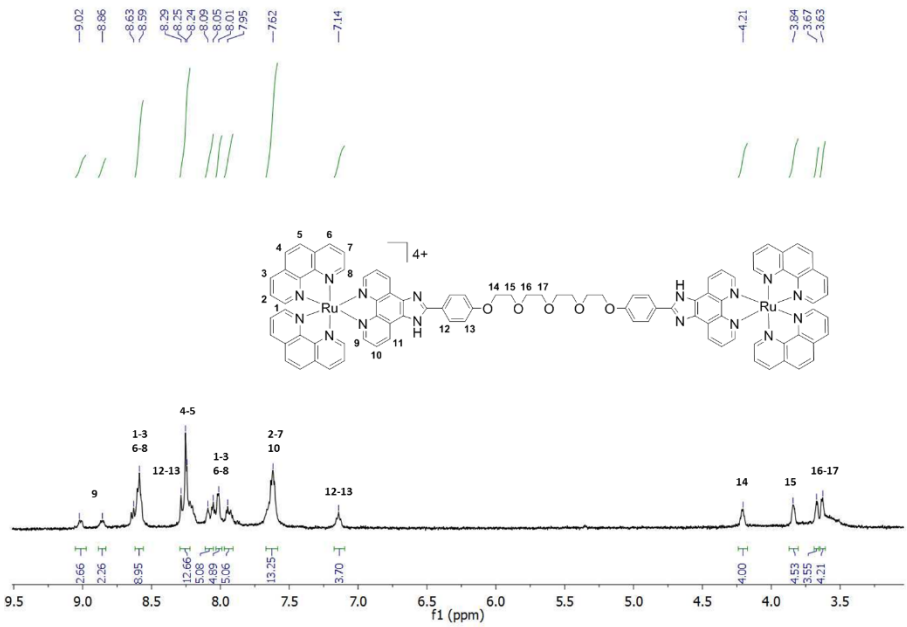

Figure S3: ^{1}H NMR spectra of **1c** (500 MHz, CD_3CN).

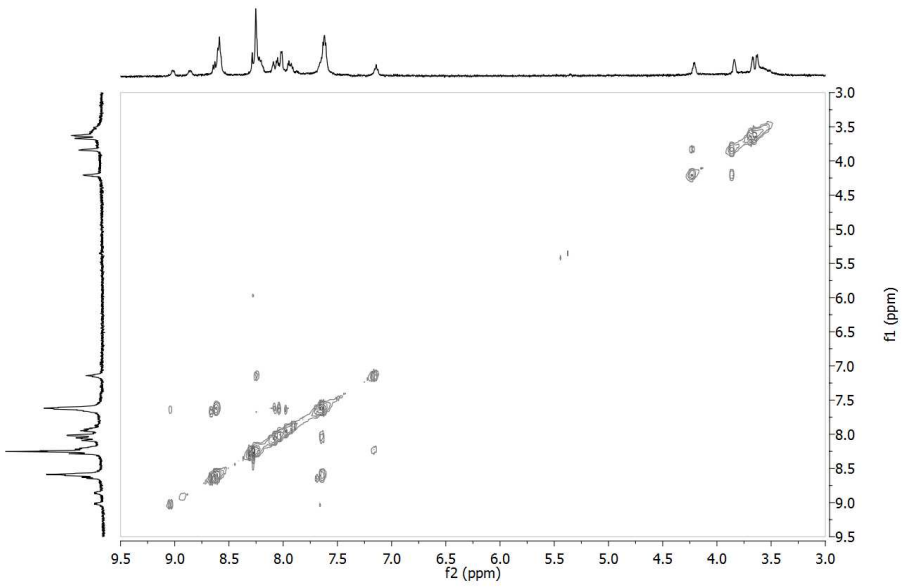

Figure S4: COSY ^{1}H- ^{1}H NMR spectra of **1c** (500 MHz, CD_3CN).

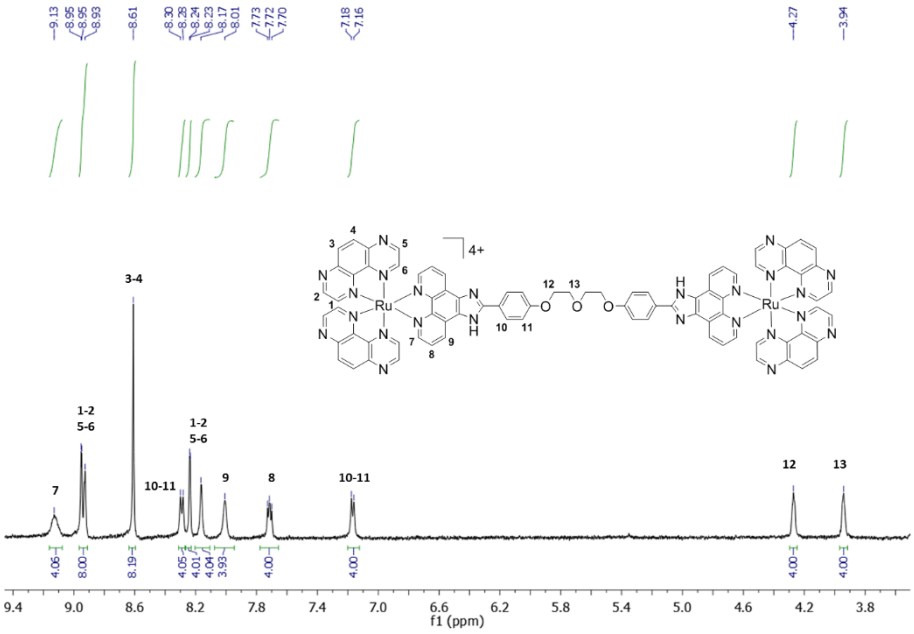

Figure S5: ^{1}H NMR spectra of **2a** (500 MHz, CD_3CN).

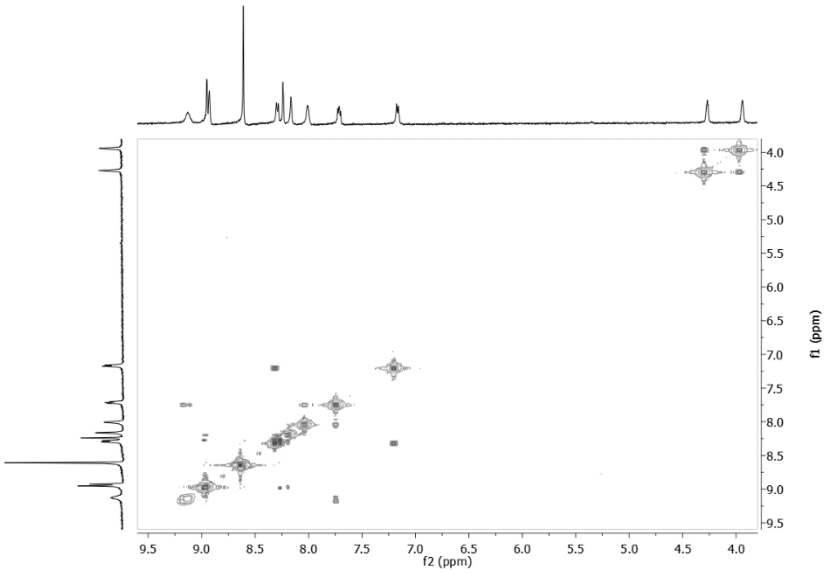

Figure S6: COSY ^{1}H-^{1}H NMR spectra of **2a** (500 MHz, CD_3CN).

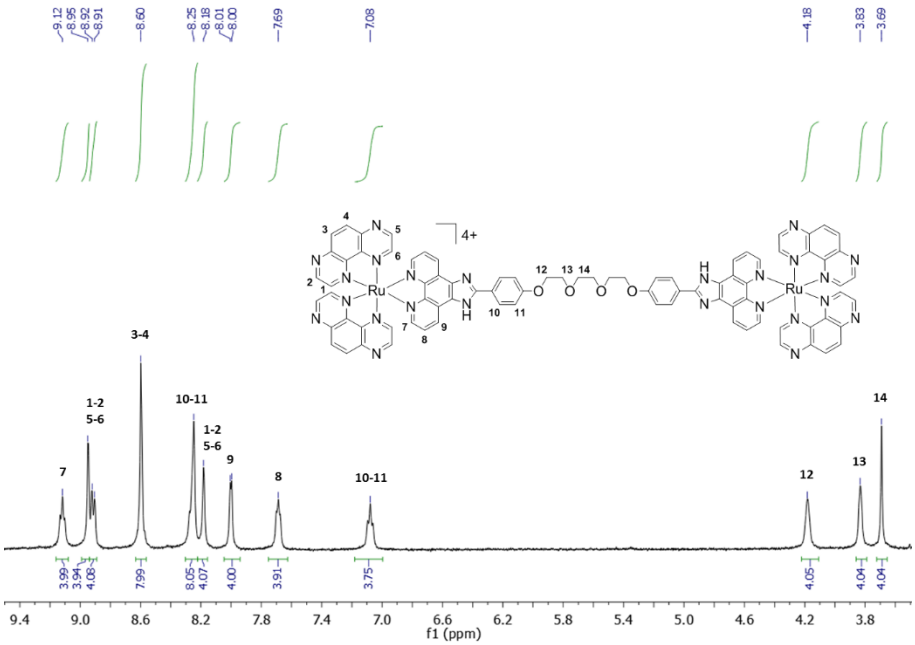

Figure S7: ^{1}H NMR spectra of **2b** (500 MHz, CD_3CN).

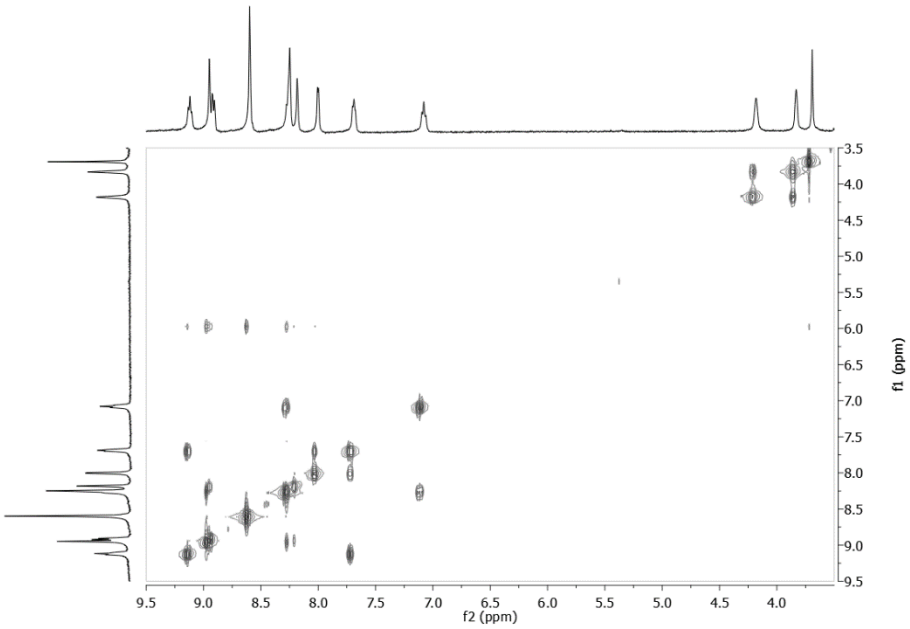

Figure S8: COSY ^{1}H-^{1}H NMR spectra of **2b** (500 MHz, CD_3CN).

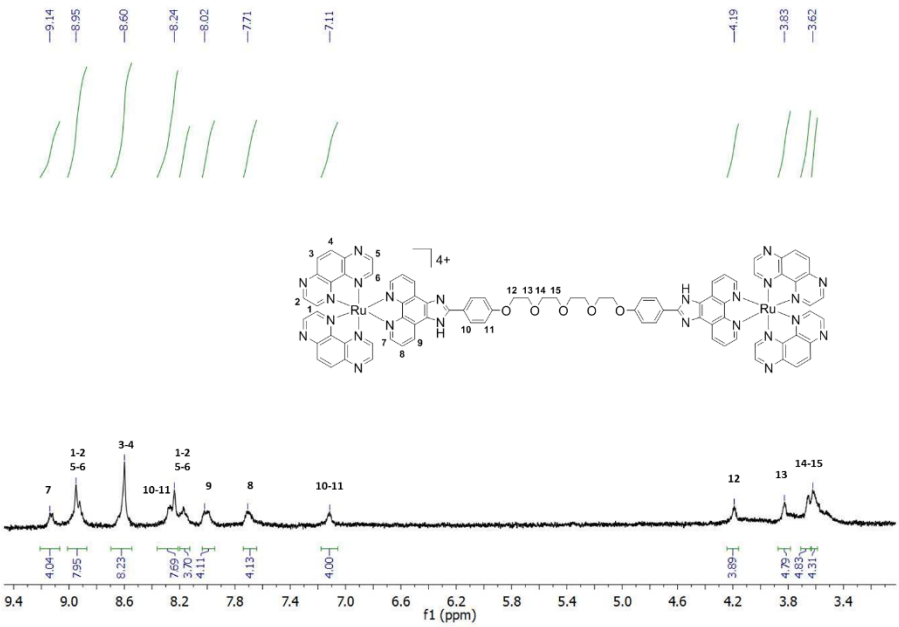

Figure S9: ^{1}H NMR spectra of **2c** (500 MHz, CD_3CN).

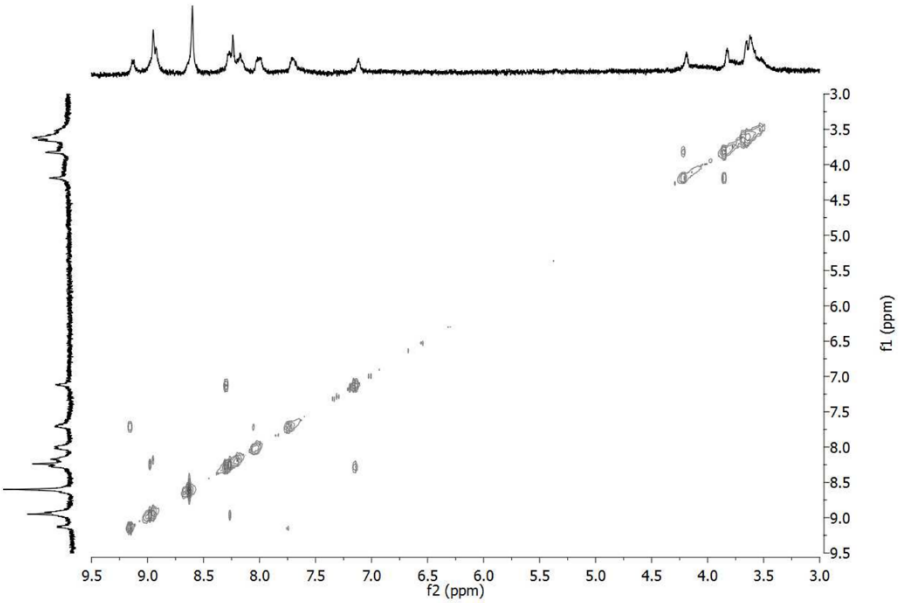

Figure S10: COSY ^{1}H-^{1}H NMR spectra of **2c** (500 MHz, CD_3CN).

4. HRMS analysis of dinuclear Ru(II) complexes

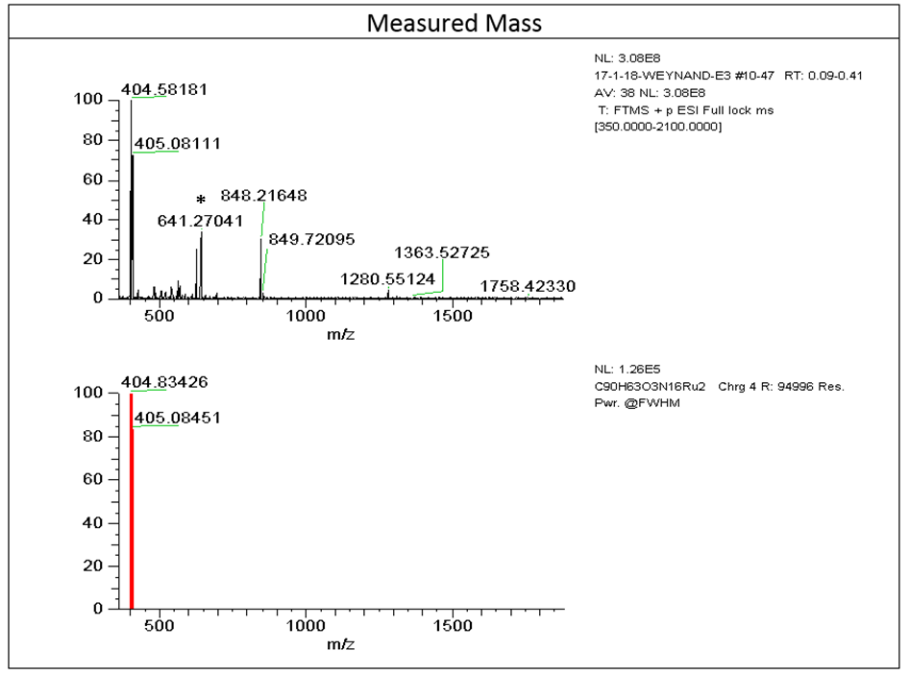

Elemental Composition Results

m/z	Formula	Score	Delta ppm	OriginalFormula	Theo. Mass
401.83517	$C_{90}H_{63}O_3N_{16}{}^{96}Ru_2$	0.00	0.48	C90H63O3N16[96]Ru2	401.83498

Figure S11: HRMS data for **1a**. *Peak of reserpine as internal standard.

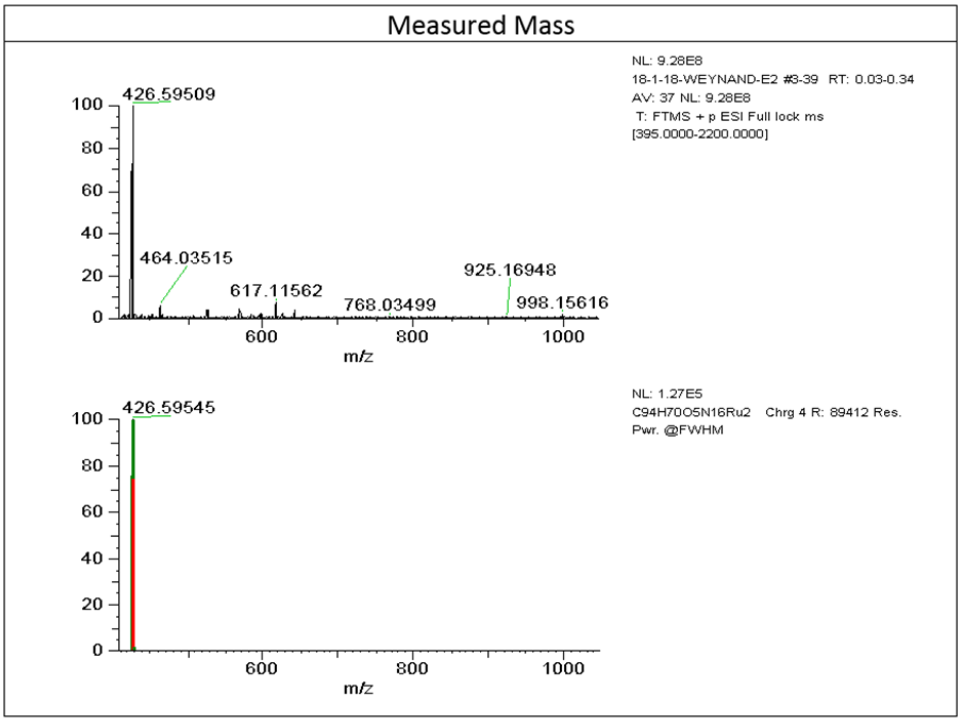

Elemental Composition Results

m/z	Formula	Score	Delta ppm	OriginalFormula	Theo. Mass
423.59713	$C_{94}H_{70}O_5N_{16}{}^{96}Ru_2$	8.50	2.37	C94H70O5N16[96]Ru2	423.59613

Figure S12: HRMS data for **1c**.

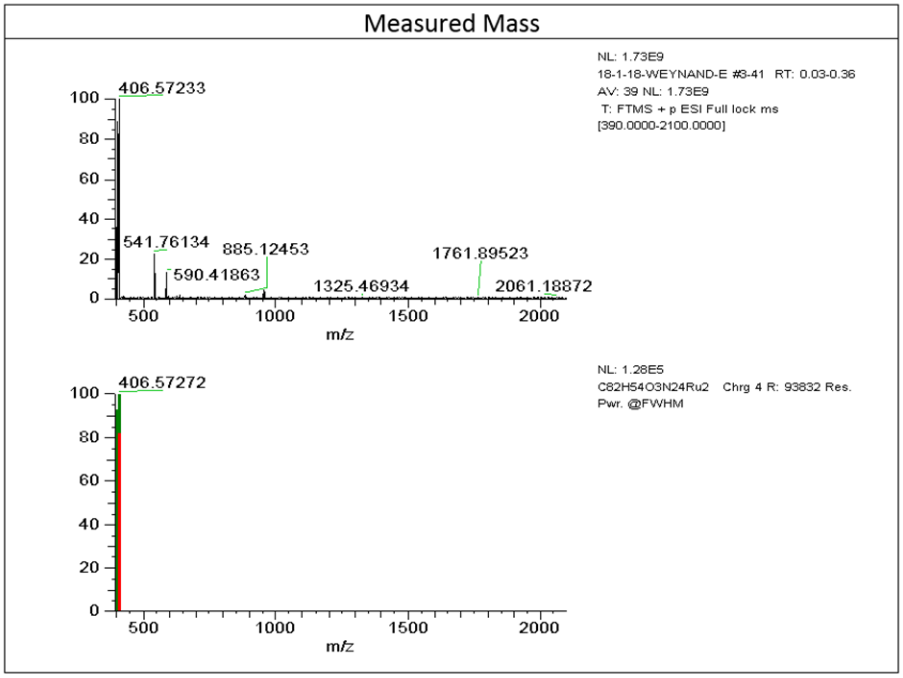

Elemental Composition Results

m/z	Formula	Score	Delta ppm	OriginalFormula	Theo. Mass
403.57480	$C_{82}H_{54}O_3N_{24}{}^{96}Ru_2$	2.53	3.18	C82H54O3N24[96]Ru2	403.57352

Figure S13: HRMS data for **2a**.

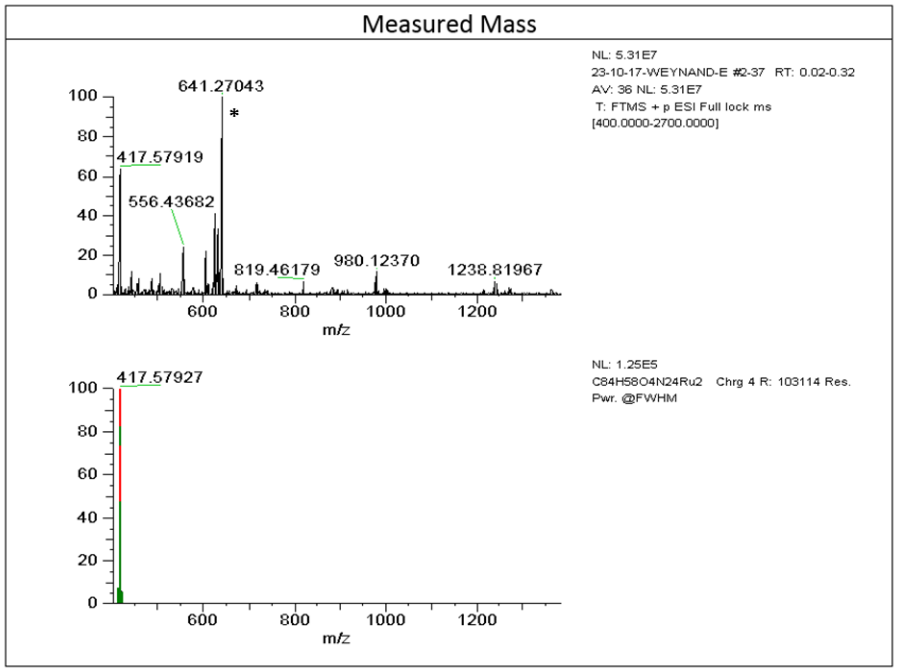

Elemental Composition Results

m/z	Formula	Score	Delta ppm	OriginalFormula	Theo. Mass
414.58049	$C_{84}H_{58}O_4N_{24}{}^{96}Ru_2$	48.01	1.01	C84H58O4N24[96]Ru2	414.58007

Figure S14: HRMS data for **2b**. *Peak of reserpine as internal standard.

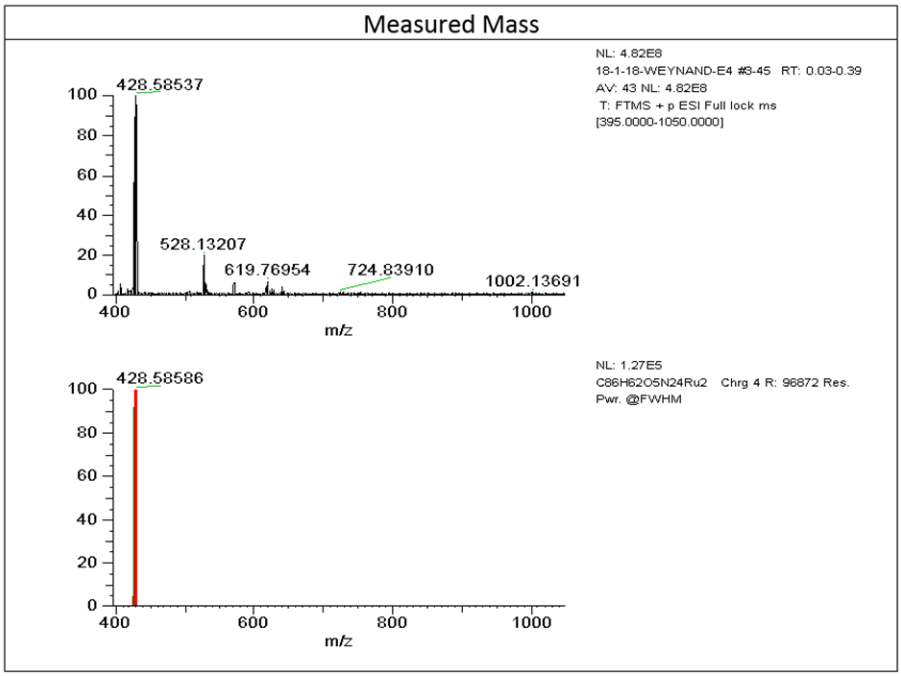

Elemental Composition Results

m/z	Formula	Score	Delta ppm	OriginalFormula	Theo. Mass
425.58760	$C_{86}H_{62}O_3N_{24}{}^{96}Ru_2$	0.00	2.29	C86H62O5N24[96]Ru2	425.58663

Figure S15: HRMS data for **2c**.

5. Absorption and emission spectra of dinuclear Ru(II) complexes

UV-vis absorption spectra were recorded on a Shimadzu UV-1700. The concentration of the complexes was 10 μM. Room temperature luminescence spectra were recorded on a Varian Cary Eclipse instrument. Luminescence intensity at 77 K was recorded on a FluoroLog3 FL3-22 from Jobin Yvon equipped with an 18 V 450 W Xenon Short Arc lamp and an R928P photomultiplier, using an Oxford Instrument Optistat DN nitrogen cryostat controlled by an Oxford Intelligent Temperature Controller (ITC503S) instrument. Quantum yield were obtained using $[Ru(bpy)_3]^{2+}$ as a reference.[5] Luminescence lifetime measurements were performed after irradiation at λ = 400 nm obtained by the second harmonic of a Titanium:Sapphire laser (picosecond Tsunami laser spectra physics 3950-M1BB+39868-03 pulse picker doubler) at a 80 kHz repetition rate. The Fluotime 200 from AMS technologies was used for the decay acquisition. It consists of a GaAs microchannel plate photomultiplier tube (Hamamatsu model R3809U-50) followed by a time-correlated single photon counting system from Picoquant (PicoHarp300). The ultimate time resolution of the system is close to 30 ps. Luminescence decays were analysed with FLUOFIT software available from Picoquant.

Table S1. Absorption and luminescence data for complexes **1a-c** and **2a-c**.

Complex	λ_{Abs} (ε) [a]	λ_{Em} [b]			Φ_{Em} [c]		τ (ns) [d]	
	CH_3CN	CH_3CN	H_2O	77K	CH_3CN	H_2O	CH_3CN	H_2O
1a	460 (3.09)	592	598	574	0.011 (0.072)	0.07 (0.92)	111 (601)	685 (1021)
1b	460 (2.77)	592	598	574	0.012 (0.069)	0.118 (0.007)	118 (515)	711 (1173)
1c	460 (2.57)	592	598	574	0.010 (0.066)	0.069 (0.011)	125 (551)	708 (1060)
2a	430 (3.20)	620	632	601	0.0058 (0.0085)	0.0018 (0.0022)	133 (150)	198 (297)
2b	430 (3.41)	620	632	601	0.0053 (0.0074)	0.0049 (0.006)	132 (143)	308 (418)
2c	430 (2.52)	620	632	601	0.0068 (0.011)	0.0034 (0.0039)	236 (232)	479 (543)

[a] λ in nm for the most bathochromic transition in MeCN (extinction coefficient, $\varepsilon x10^4$ $M^{-1}cm^{-1}$). [b] λ in nm at RT in MeCN and H_2O and at 77K in MeOH/ EtOH 4/1. [c] Quantum yield of emission measured by comparison with the reference $[Ru(bpy)_3]^{2+}$, under air and under argon (in brackets), excitation at 450 nm, errors are estimated as 10%.[5] [d] Luminescence lifetime (after irradiation at λ=400 nm) measured under air and under argon (in brackets); errors are estimated as 5%.

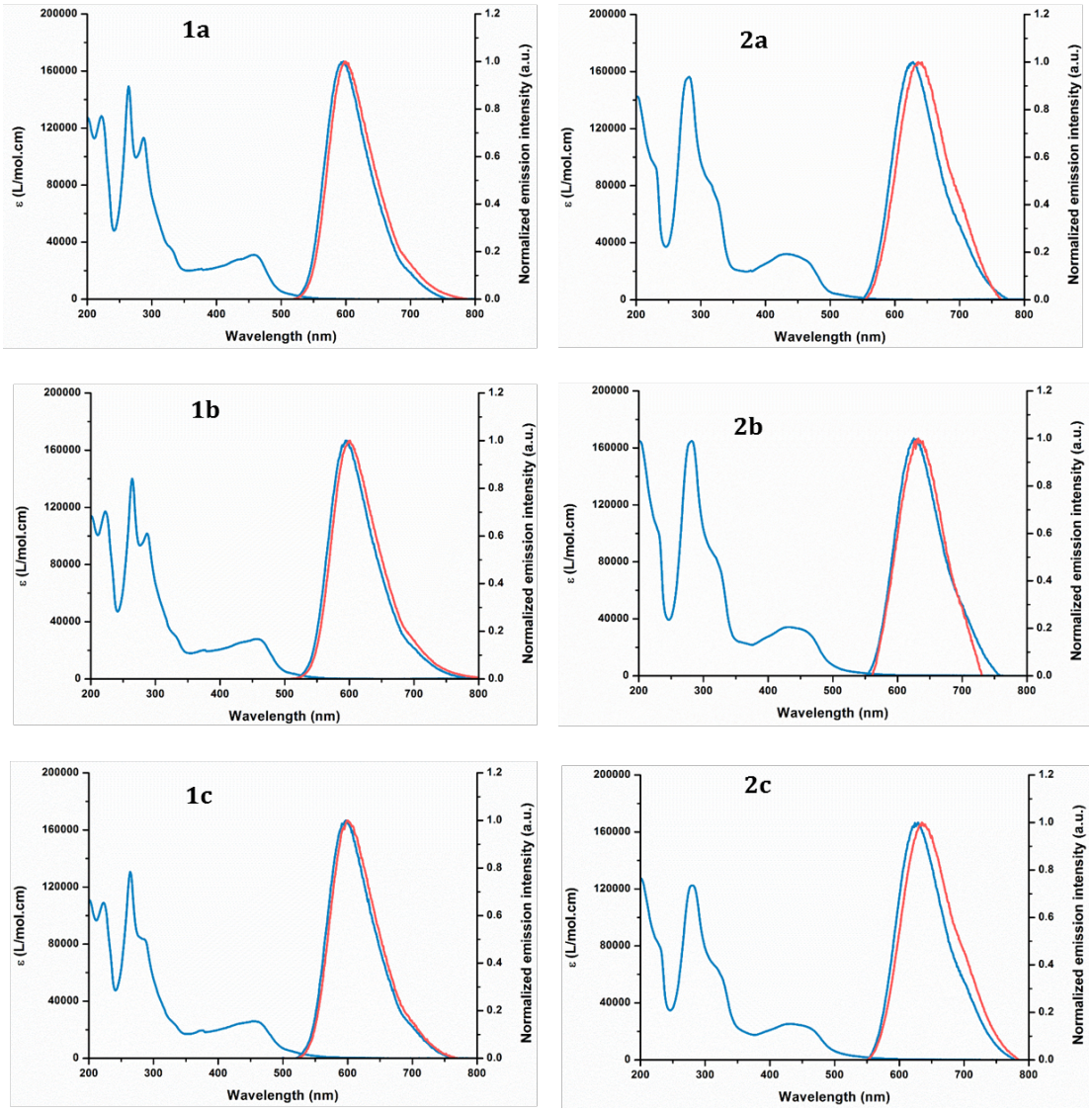

Figure S16: Absorption and emission spectra under air in acetonitrile (blue) and in water (red) for **1a-c** and **2a-c**.

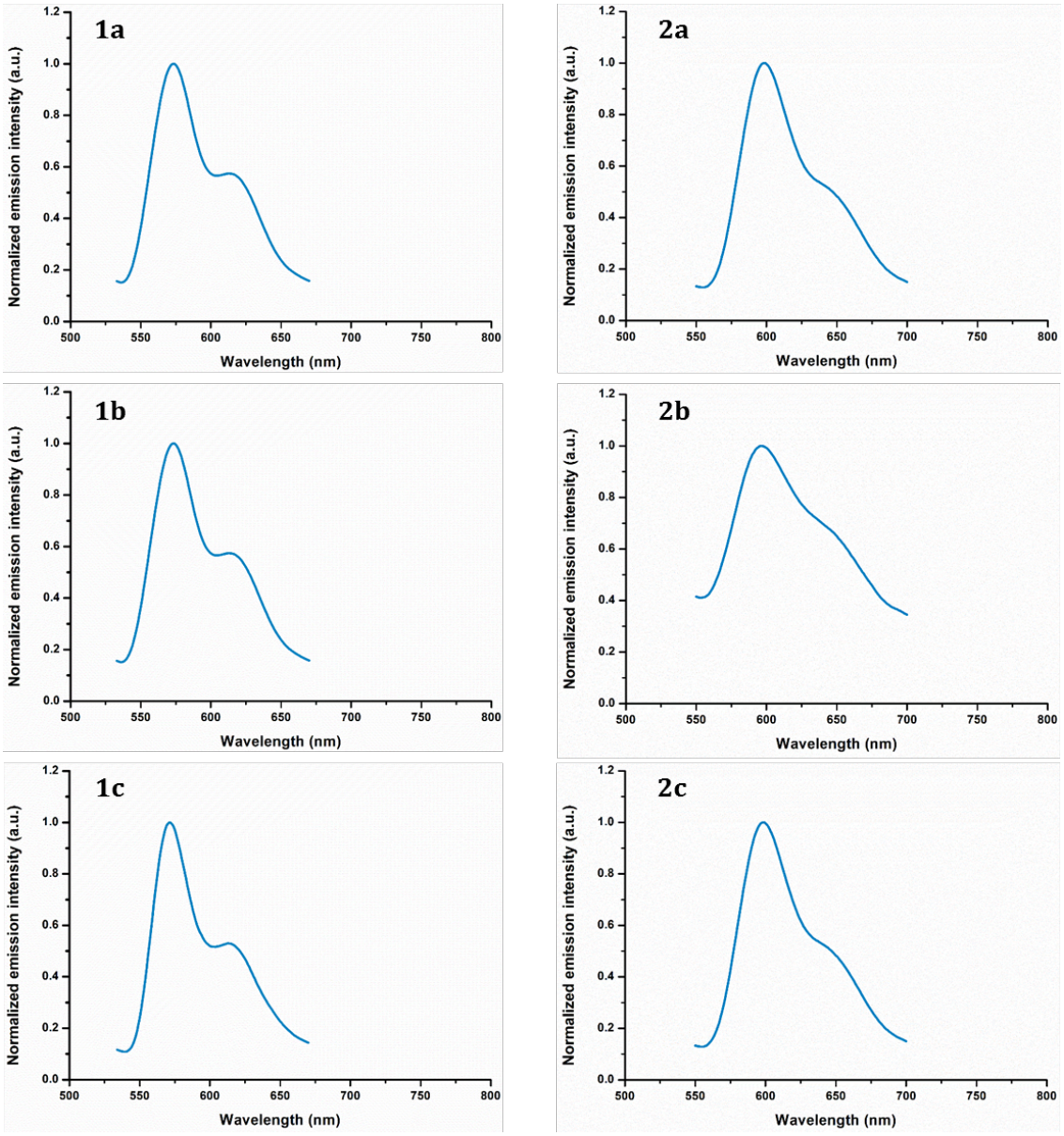

Figure S17: Emission spectra under air at 77K in EtOH/ MeOH (4/1, v/v) for **1a-c** and **2a-c**.

6. Cyclic voltammograms of dinuclear Ru(II) complexes

Cyclic voltammetry was carried out in a one-compartment cell, using a glassy carbon disk working electrode (approximate area = 0.03 cm^2), a platinum wire counter electrode, and an Ag/AgCl reference electrode. The potential of the working electrode is controlled by an Autolab PGSTAT 100 potentiostat through a PC interface. The cyclic voltammograms were recorded with a sweep rate of 100 mVs^{-1}, in dried acetonitrile (Sigma-Aldrich, HPLC grade). The concentration of the complexes was 8.10^{-4} mol/L, with 0.1 mol/L tetrabutylammonium perchlorate as supporting electrolyte. Before each measurement, the samples were purged with nitrogen. Redox potentials were controlled by comparison with ferrocene, added at the end of the measurement.

Table S2. Absorption and luminescence data for complexes **1a-c** and **2a-c**.

Complex	$E_{ox\ 1/2}$	E^*_{ox} [a]	$E_{red\ 1/2}$	E^*_{red} [a]
1a-c	+1.39	-0.71	-1.40	+0.70
2a-c	+1.81	-0.19	-0.73	+1.27

Data were measured at room temperature in MeCN with 0.1M Bu_4NClO_4 as the supporting electrolyte (V *vs.* Ag/AgCl), complexes concentration = 0.8 mM, [a] Excited state potentials estimated from equations E*ox= E½ ox - E0-0 and E*red= E½ red + E0-0. The energy of the excited state, E0-0, was assimilated to the maximum of the emission spectrum in acetonitrile at 298 K.

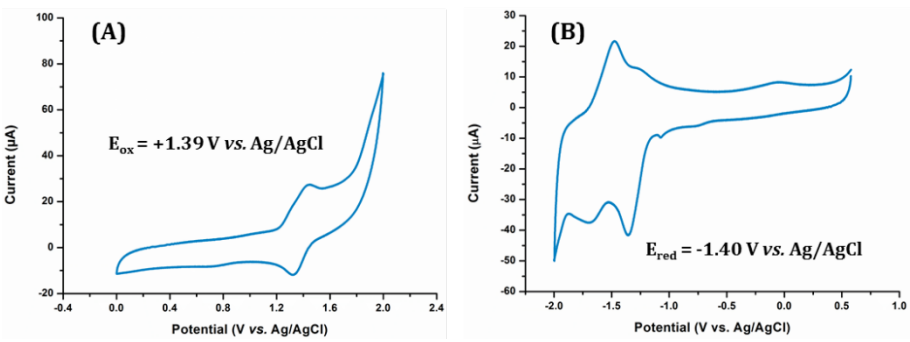

Figure S18: Cyclic voltammograms of **1a**. (A) positive polarization and (B) negative polarization.

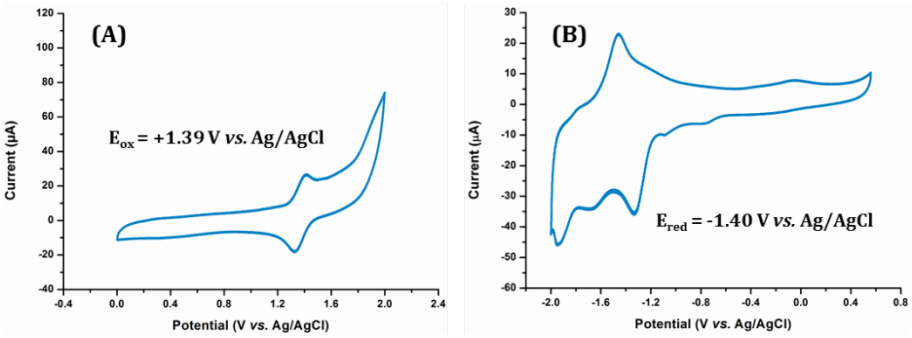

Figure S19: Cyclic voltammograms of **1b**. (A) positive polarization and (B) negative polarization.

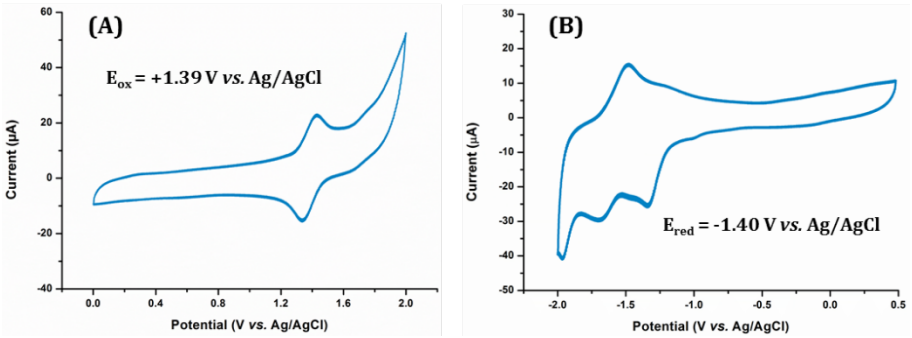

Figure S20: Cyclic voltammograms of **1c**. (A) positive polarization and (B) negative polarization.

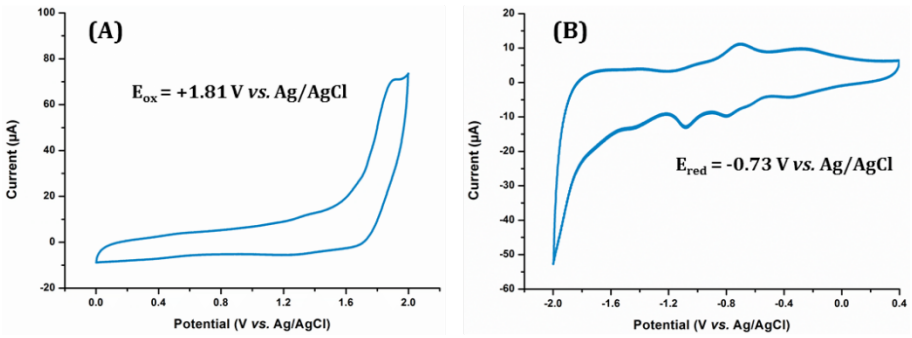

Figure S21: Cyclic voltammograms of **2a**. (A) positive polarization and (B) negative polarization.

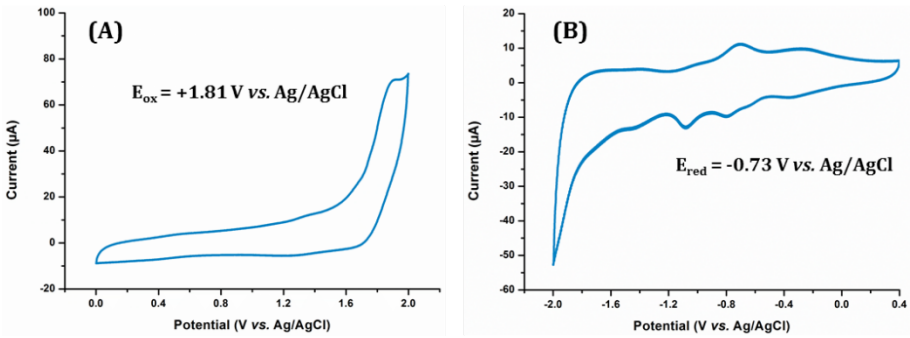

Figure S22: Cyclic voltammograms of **2b**. (A) positive polarization and (B) negative polarization.

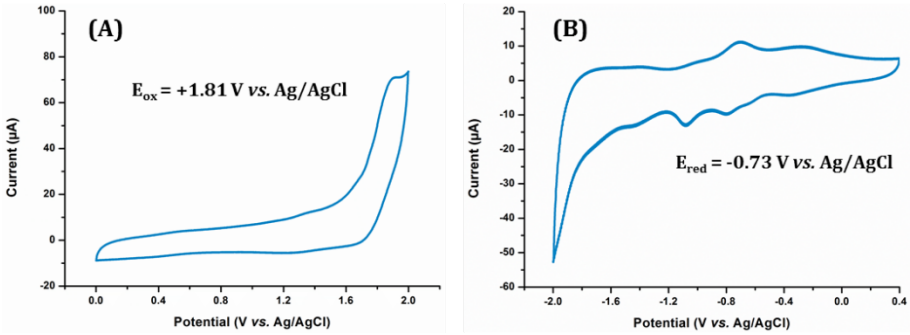

Figure S23: Cyclic voltammograms of **2c**. (A) positive polarization and (B) negative polarization.

7. Luminescence quenching by dGMP

dGMP titration experiment of complexes were recorded on a Varian Cary Eclipse instrument. A solution of dGMP (0.5 M) was progressively added to a solution of complex (25 μM) in 50 mM Tris-HCl buffer, pH = 7.4.

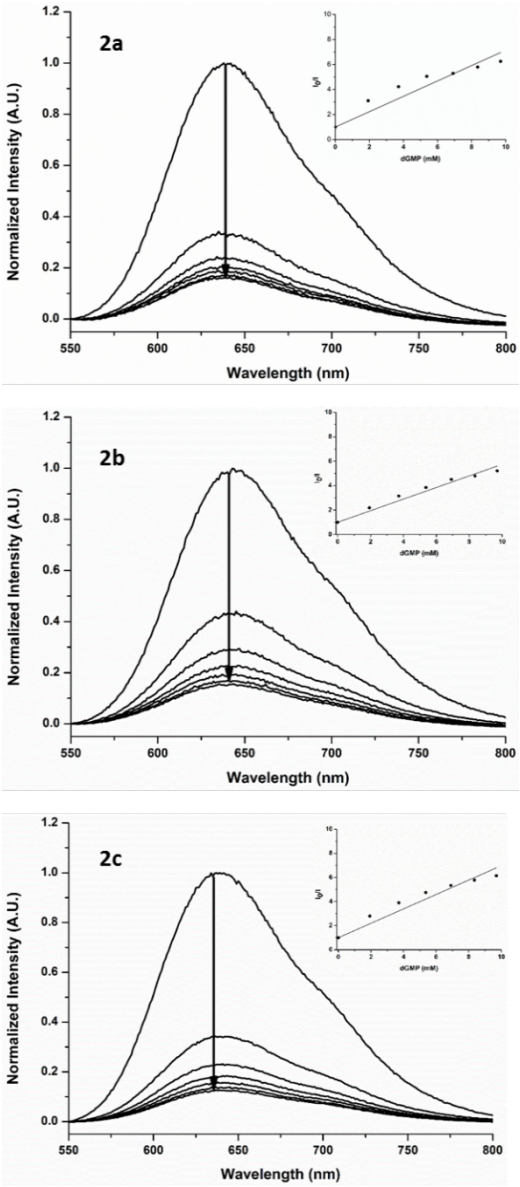

Figure S24: Emission spectra of complexes **2a-c** in the presence of increasing concentrations of dGMP, inset: Stern-Volmer plot. Complex concentration: 25 μM in Tris-HCl buffer (50 mM at pH 7.4). Addition of dGMP from 0 mM to 10 mM. Excitation at λ = 430 nm. Quenching rate constant (kq) were obtained using the Stern–Volmer equation $I_0/I = 1 + k_{qT0}[dGMP]$. I_0/I (where I_0 is the luminescence of the complex in the absence of a quencher, here dGMP, and I is the luminescence in the presence of dGMP) as a function of the quencher concentration

8. Circular dichroism spectroscopic studies

Prior to CD analysis, the oligonucleotides were annealed by heating the sample at 95°C for 5 min in buffer (10 mM Tris buffer pH 7.04) with 100 mM NaCl or KCl for both **G1** and **G2T1**. Analyses were recorded on a Jasco J-810 spectro-polarimeter using 1 cm length quartz cuvette. Spectra were recorded in a range of 5 from 25°C to 90°C with a wavelength range of 220 to 330 nm. For each temperature, the spectrum was an average of three scans with a 0.5 s response time, a 1 nm data pitch, a 4 nm bandwidth and a 200 nm min^{-1} scanning speed. Melting temperatures were obtained using Boltzmann fit on Origin soft-ware. Each curve fit was only accepted with r>0.99.

Table S3: Variation of the melting temperatures (ΔTm, °C) from CD melting curves of G2T1 and G1 in the presence of **1a-c** and **2a-c**.

DNA structures	Buffer	1a	1b	1c	2a	2b	2c
G2T1	Na^+	+7.5	+8.2	+5.8	+6.4	+1.3	+4.2
	K^+	+2.5	+2.0	+6.2	+2.1	-0.2	+2.4
G1	Na^+	-2.5	-0.1	+0.1	+1.3	+1.4	+1.3
	K^+	-1.6	-4.9	-2.2	-0.2	+1.2	+1.2

Measurements were performed in Tris-HCl 10 mM, NaCl or KCl 100 mM (pH 7.04). The amount of complex added was such that all samples had a 2:1 ratio of Ru(II) centre with respect to each G-quadruplex unit (e.g., [**1a**]:[G1]=1:1; [**2a**]:[G2T1]=2:1). Error is estimated to 1°C.

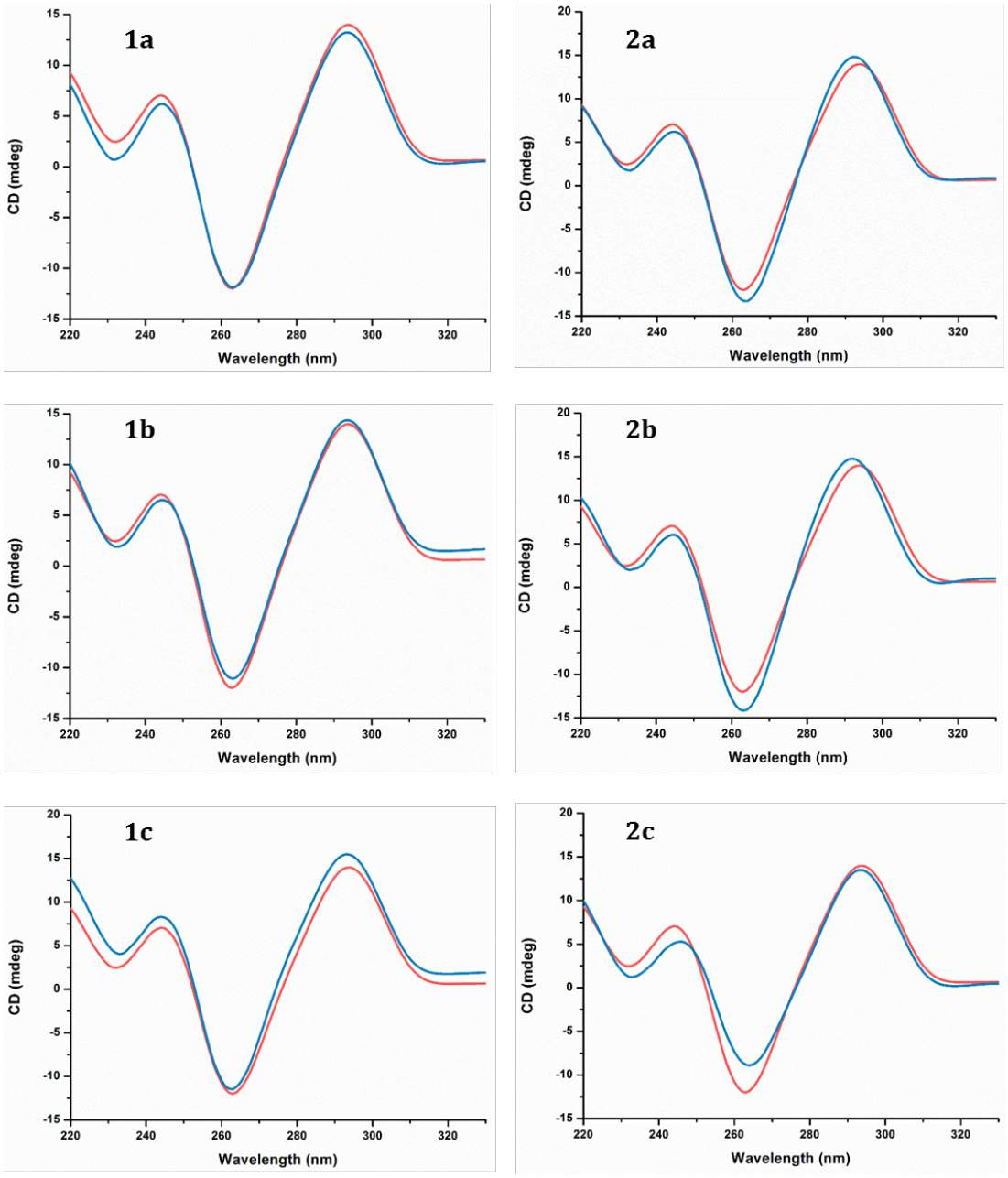

Figure S25: CD spectra at 20°C of 1 equiv. (2.5 µM) in G2T1 (in red) in sodium buffer (10 mM Tris-HCl, 100 mM NaCl, pH=7.04) in presence of 2 equiv. of complexes (in blue) **1a-c** and **2a-c**.

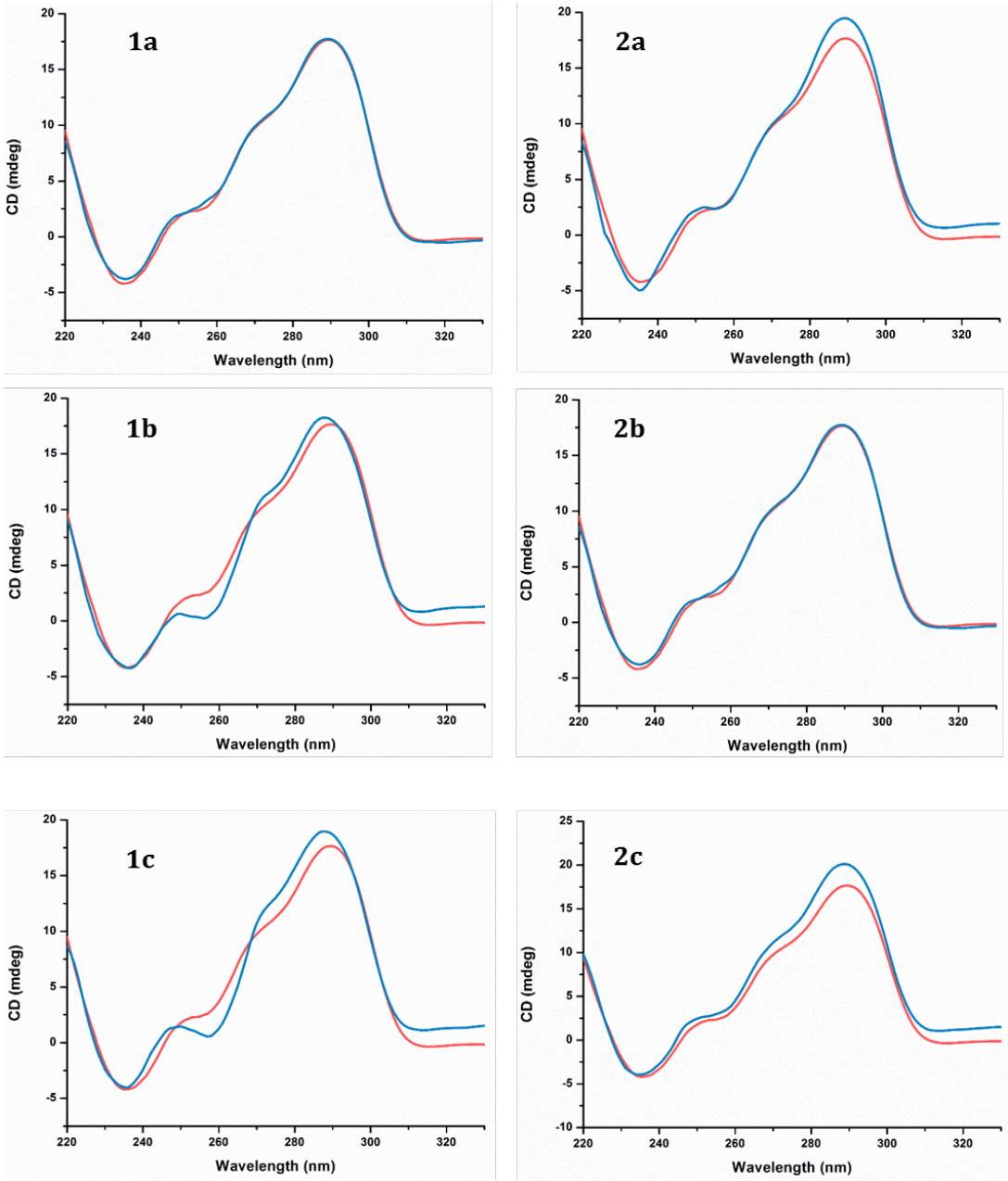

Figure S26: CD spectra at 20°C of 1 equiv. (2.5 μM) in G2T1 (in red) in potassium buffer (10 mM Tris-HCl, 100 mM KCl, pH=7.04) in presence of 2 equiv. of complexes (in blue) **1a-c** and **2a-c**.

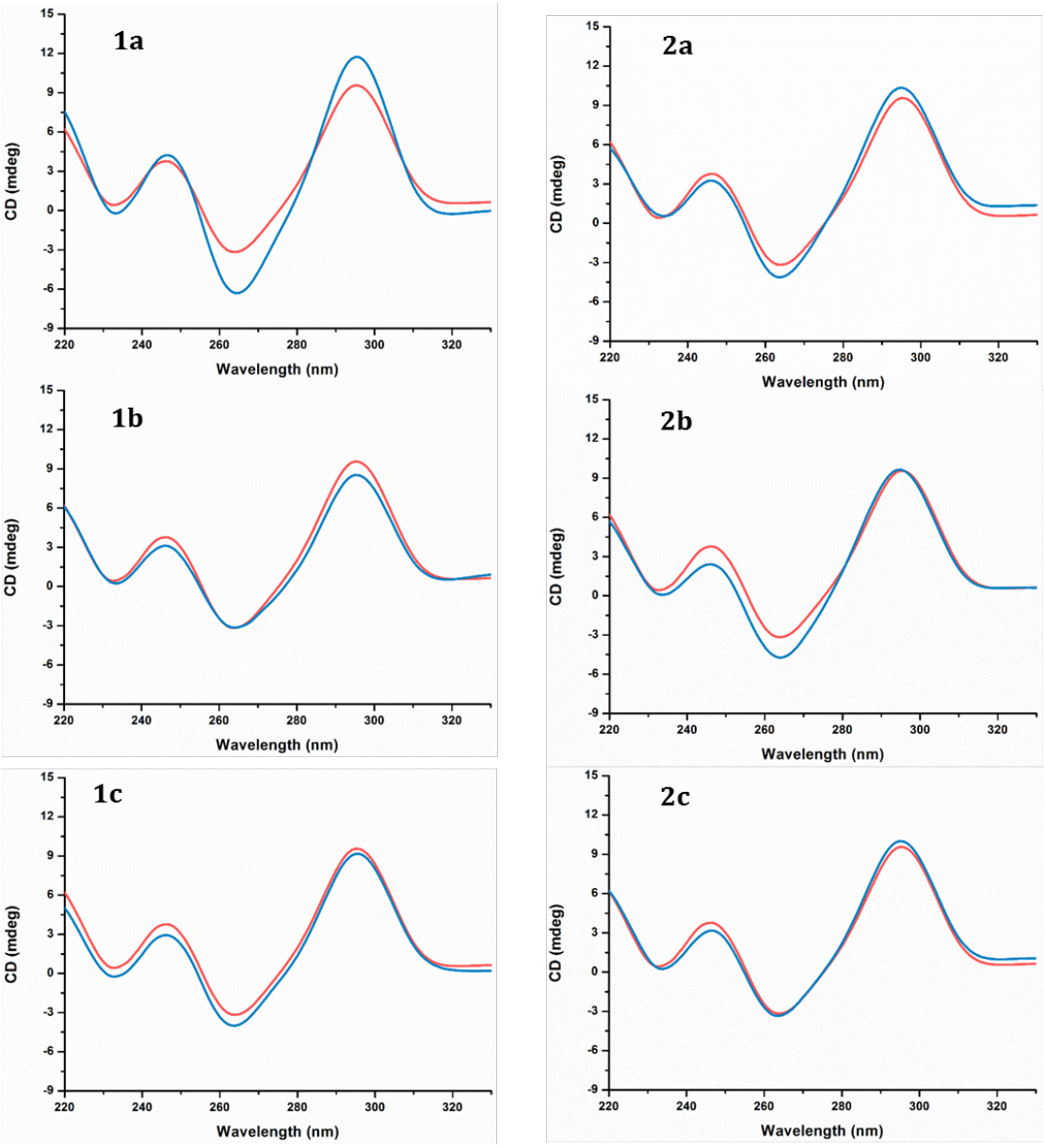

Figure S27: CD spectra of 1 equiv. (2.5 μM) in G1 (in red) in sodium buffer (10 mM Tris-HCl, 100 mM NaCl, pH=7.04) in presence of 2 equiv. of complexes (in blue) **1a-c** and **2a-c**.

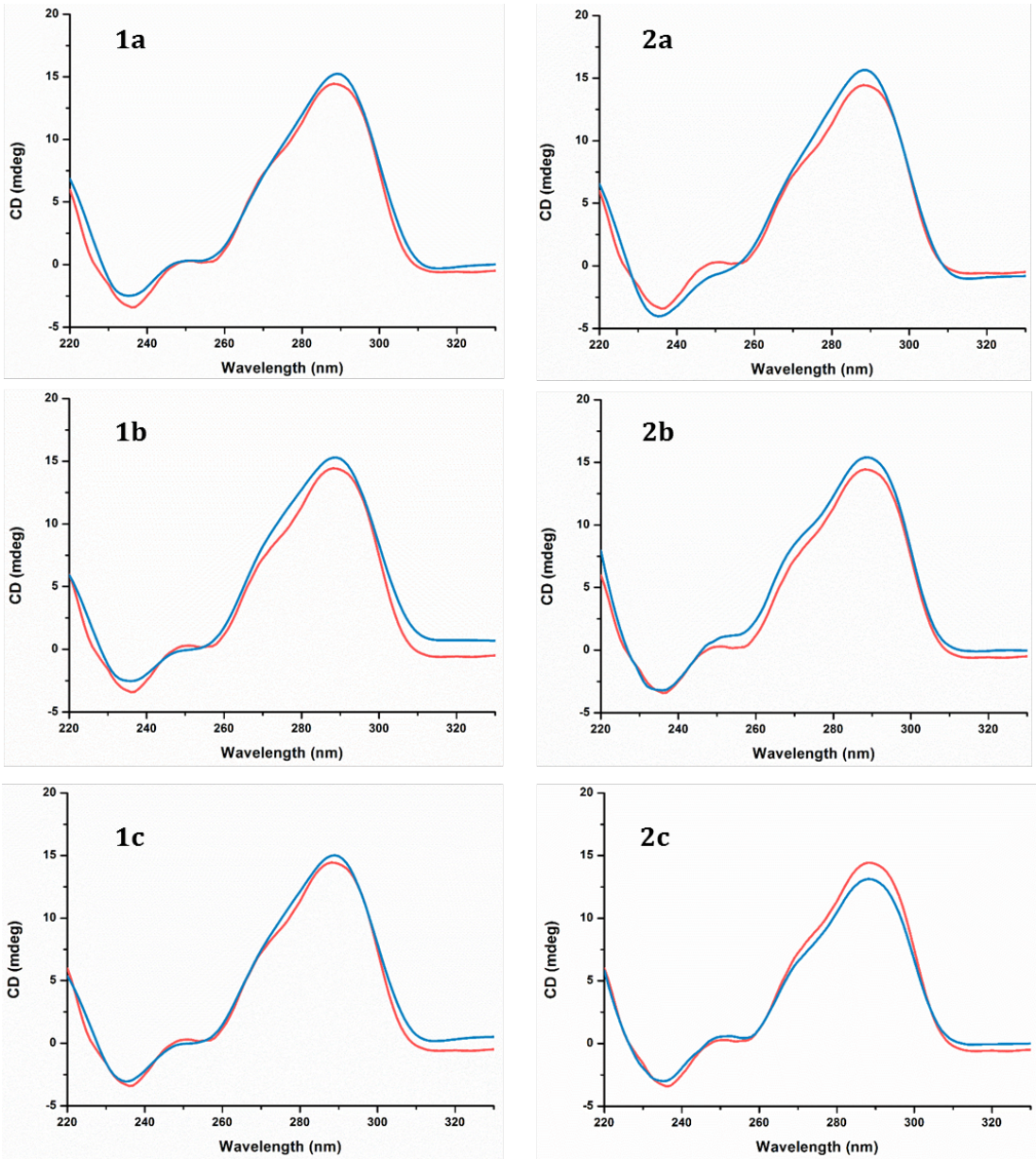

Figure S28: CD spectra of 1 equiv. (2.5 μM) in G1 (in red) in potassium buffer (10 mM Tris-HCl, 100 mM KCl, pH=7.04) in presence of 2 equiv. of complexes (in blue) **1a-c** and **2a-c**.

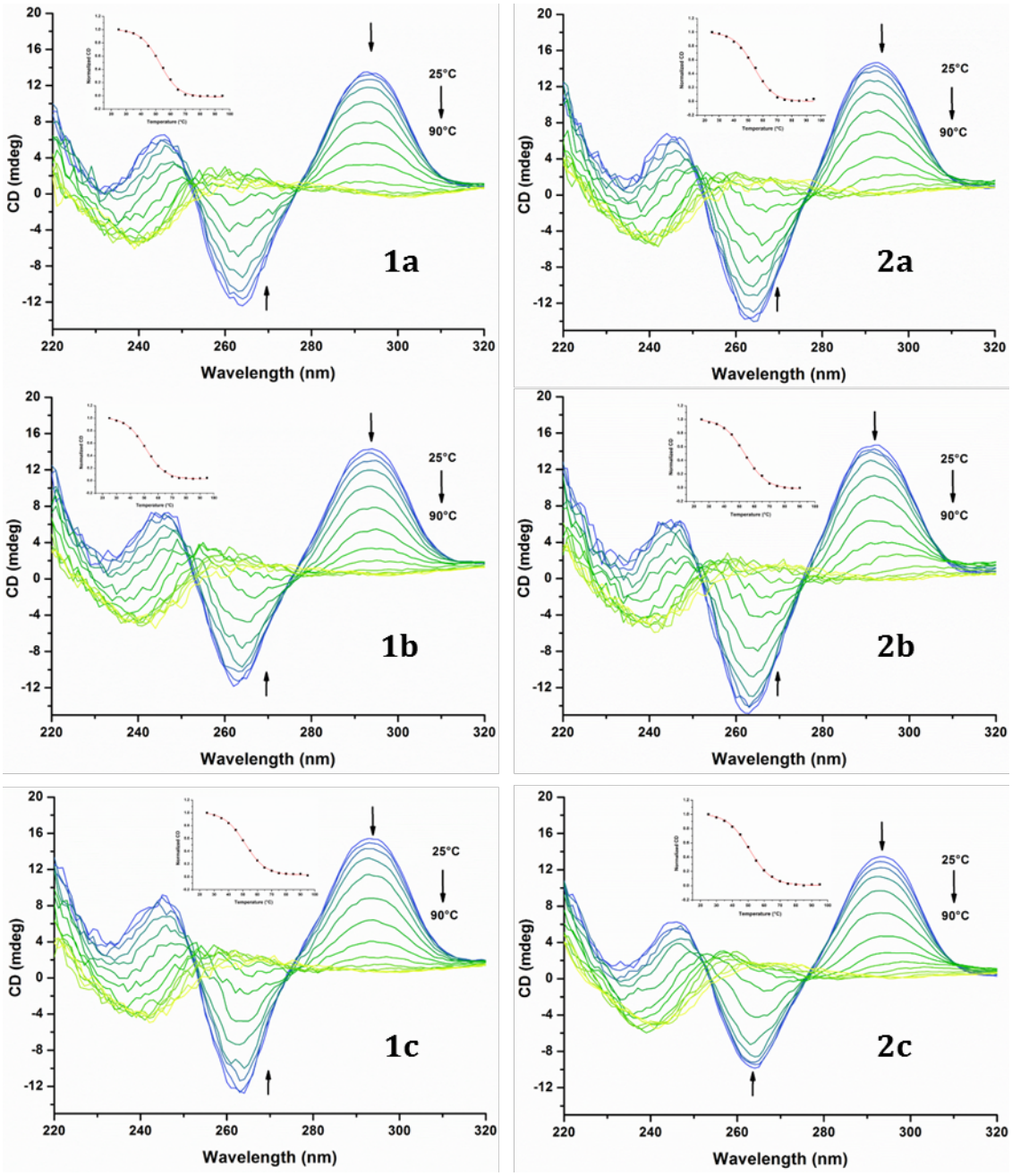

Figure S29: CD spectra upon increasing temperatures and melting curves (inset) of G2T1 (1 eq., 2.5 μM) in the presence of 2 eq. of complexes **1a-c** and **2a-c** in a sodium buffer (10 mM Tris-HCl, 100 mM KCl, pH=7.04).

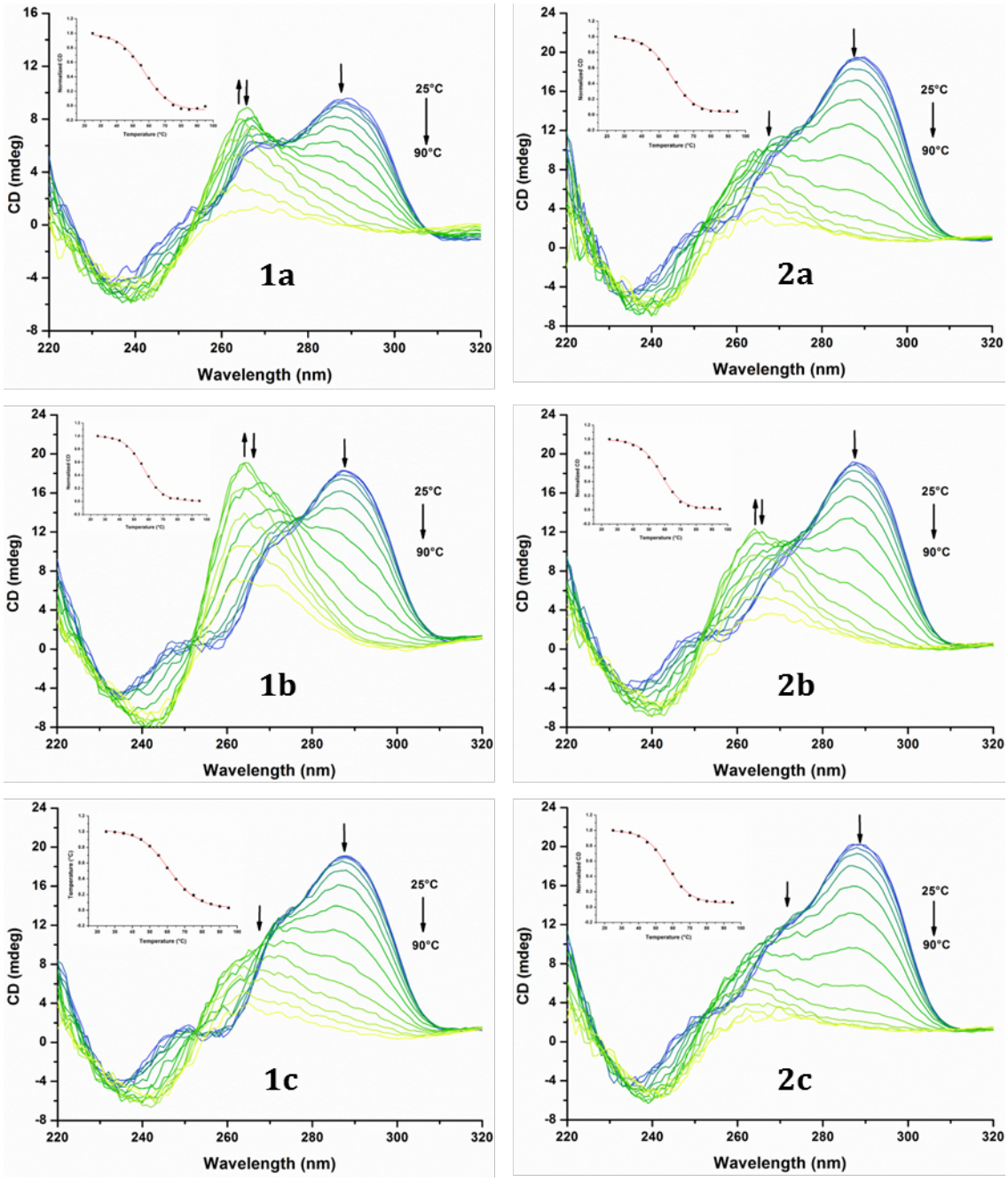

Figure S30: CD spectra upon increasing temperatures and melting curves (inset) of G2T1 (1 eq., 2.5 μM) in the presence of 2 eq. of complexes **1a-c** and **2a-c** in a potassium buffer (10 mM Tris-HCl, 100 mM KCl, pH=7.04).

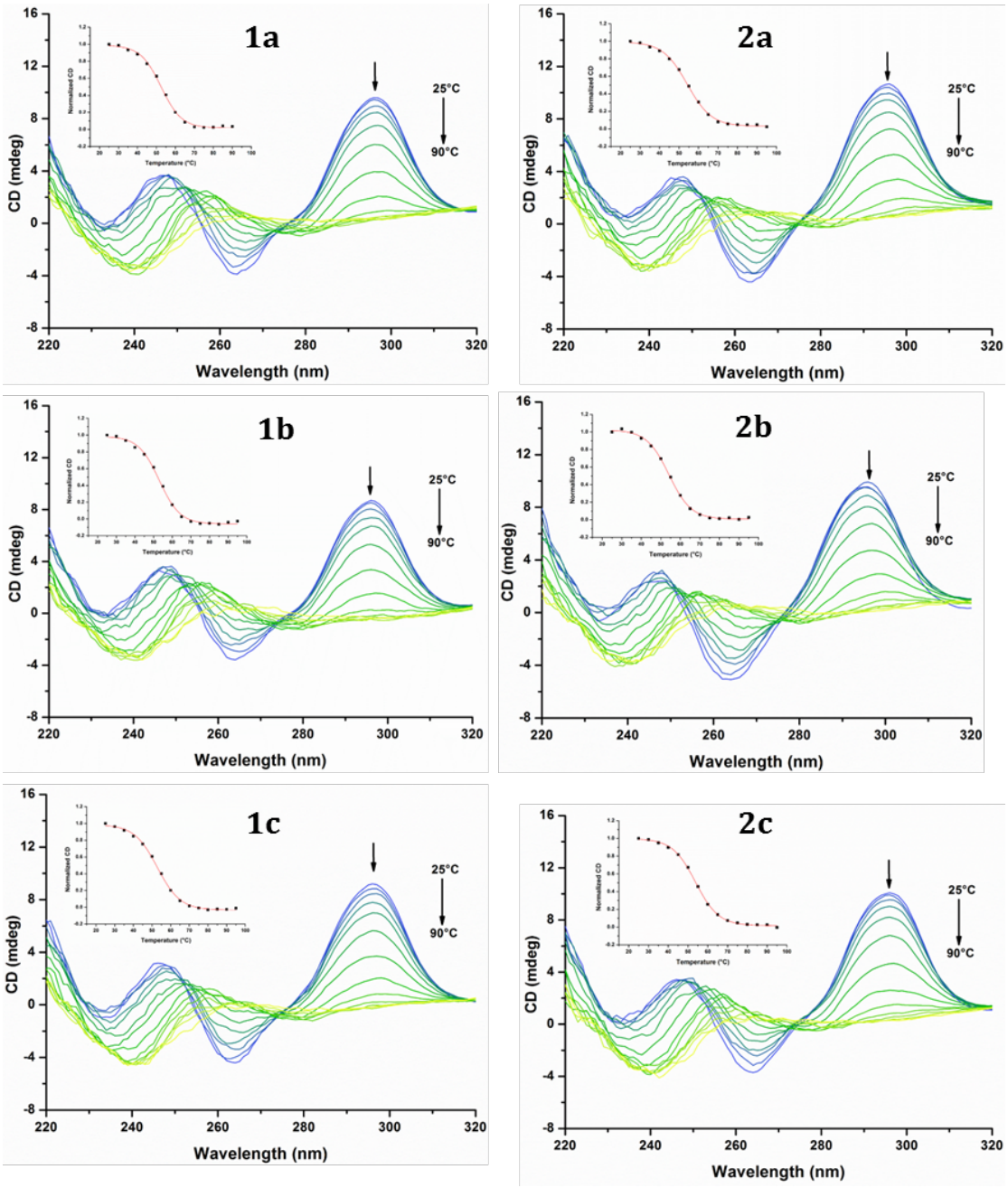

Figure S31: CD spectra upon increasing temperatures and melting curves (inset) of G1 (1 eq., 2.5 μM) in the presence of 2 eq. of complexes **1a-c** and **2a-c** in a sodium buffer (10 mM Tris-HCl, 100 mM NaCl, pH=7.04).

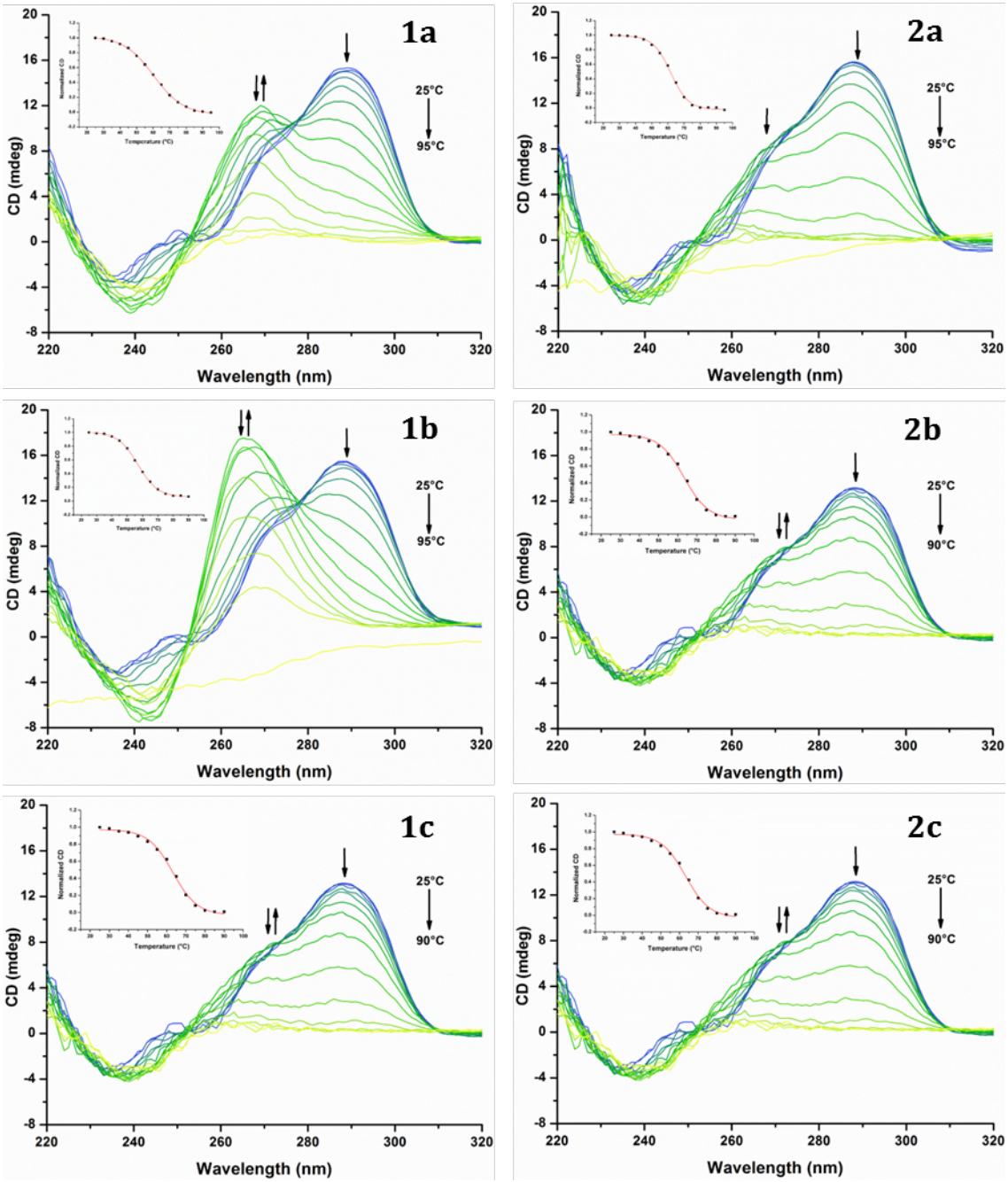

Figure S32: CD spectra upon increasing temperatures and melting curves (inset) of G1 (1 eq., 2.5 μM) in the presence of 2 eq. of complexes **1a-c** and **2a-c** in a potassium buffer (10 mM Tris-HCl, 100 mM KCl, pH=7.04).

9. BLI binding analysis

Heterogeneous model

The data were fitted using a heterogeneous ligand model and two interactions were processed as described below:

$$A + B_1 \rightleftharpoons AB_1 \quad \text{(eq.}\mathbf{1}\text{)}$$
$$A + B_2 \rightleftharpoons AB_2$$
(eq.**2**)

where *A*, Analyte (G quadruplex dimeric, monomeric or DNA duplex); B_1, G4-target interaction site; AB_1, first complex; and B_2, 2nd interaction site of G4-target or $B_2 = AB_1$; AB_2, second complex.

The equations used are:

$$\frac{dA}{dt} = \left(tc\,\sqrt[3]{f}\,(C - A)\right) - \left(k_{on1}\,A\,B_1 - k_{off1}\,AB_1\right) - \left(k_{on2}\,A\,B_2 - k_{off2}\,AB_2\right) \quad \text{(eq.}\mathbf{3}\text{)}$$
$$\frac{dB_1}{dt} = -(k_{on1}\,A\,B_1 - k_{off1}\,AB_1) \quad \text{(eq.}\mathbf{4}\text{)}$$
$$\frac{dB_2}{dt} = -(k_{on2}\,A\,B_2 - k_{off2}\,AB_2) \quad \text{(eq.}\mathbf{5}\text{)}$$
$$\frac{dAB_1}{dt} = (k_{on1}\,A\,B_1 - k_{off1}\,AB_1) \quad \text{(eq.}\mathbf{6}\text{)}$$
$$\frac{dAB_2}{dt} = (k_{on2}\,A\,B_2 - k_{off2}\,AB_2) \quad \text{(eq.}\mathbf{7}\text{)}$$

The first term in eq.**3** is the correction of the mass diffusion.

In order to fit, an initial value is given for the parameters, k_{on}, k_{off} and R_{max}. Finding the best match between the model and the experiment is typically achieved through regression. An estimator, c^2, is used to determine the difference between curves. The unknown parameters are allowed to vary until the minimum c^2 is reached. The fitting is performed with different initial values, and the results presented correspond to the minimal c^2 value found for each system.

We chose to report only one K_D value which corresponds to the specific interaction between the DNA structure and the ruthenium complex. This interaction was determined from the R_{max} value and after deconvolution of the signal. The second interaction was considered as non-specific interaction due to a bad compensation by the reference sensor. This interaction is 10 times weaker than the specific interaction. BLI sensors coated with streptavidin (SA sensors) were purchased from Forte Bio (PALL). Prior to use, they were immerged 10 minutes in buffer before functionalization to dissolve the sucrose layer. Reference sensors without DNA immobilization were used to subtract the non-specific adsorption on the SA layer. The sensorgrams were fitted using a heterogeneous model. The reported values are the means of representative independent experiments, and the errors provided are standard deviations from the mean. Each experiment was repeated at least two times.

Table S4: Dissociation constant (K_D) of the interaction of complexes **1a-c** and **2a-c** with DNA structures G2T1, G1 and HP GC determined by BLI experiments.

DNA structure	Constants	Complex					
		1a	1b	1c	2a	2b	2c
G2T1	k_{on} (10^5 $M^{-1}s^{-1}$)	2.5 ± 0.1	2.7 ± 0.2	4.7 ± 0.9	4.6 ± 0.4	3.9 ± 0.2	2.1 ± 1.2
	k_{off} (10^{-2} s^{-1})	3.9 ± 0.6	4.4 ± 0.5	5.6 ± 0.1	4.6 ± 0.2	8.4 ± 3.6	5.2 ± 3.6
	K_D (μM) [a]	**0,33** ± 0,14	**0,17** ± 0,01	**0,12** ± 0,02	**0,10** ± 0,02	**0,22** ± 0,10	**0,21** ± 0,05
G1	k_{on} (10^5 $M^{-1}s^{-1}$)	1.5 ± 0.5	2.1 ± 0.2	2.6 ± 2.3	4.2 ± 0.8	3.9 ± 0.5	1.3 ± 1.2
	k_{off} (10^{-2} s^{-1})	6.2 ± 1.6	5.5 ± 1.3	3.2 ± 1.9	6.6 ± 0.4	10 ± 1	8.2 ± 7.8
	K_D (μM) [a]	**0,43** ± 0,04	**0,26** ± 0,04	**0,23** ± 0,13	**0,17** ± 0,04	**0,25** ± 0,05	**0,65** ± 0,18
HP GC	k_{on} (10^4 $M^{-1}s^{-1}$)	3.0 ± 0.1	3.2 ± 0.3	7.2 ± 0.1	5.0 ± 1.5	8.7 ± 5.3	6.5 ± 1.9
	k_{off} (10^{-2} s^{-1})	4.3 ± 0.2	3.8 ± 0.3	3.4 ± 0.1	2.4 ± 0.3	3.6 ± 0.9	6.1 ± 0.9
	K_D (μM) [a]	**1,60** ± 0,05	**1,20** ± 0,25	**0,48** ± 0,02	**0,37** ± 0,05	**0,38** ± 0,04	**0,96** ± 0,14

[a] Equilibrium dissociation constants deduced from the kinetic rate constants. The errors provided are standard deviations from the mean values. The running buffer were Tris-HCl 10 mM, NaCl 100 mM (pH 7.04) and 0.5% v/v surfactant.

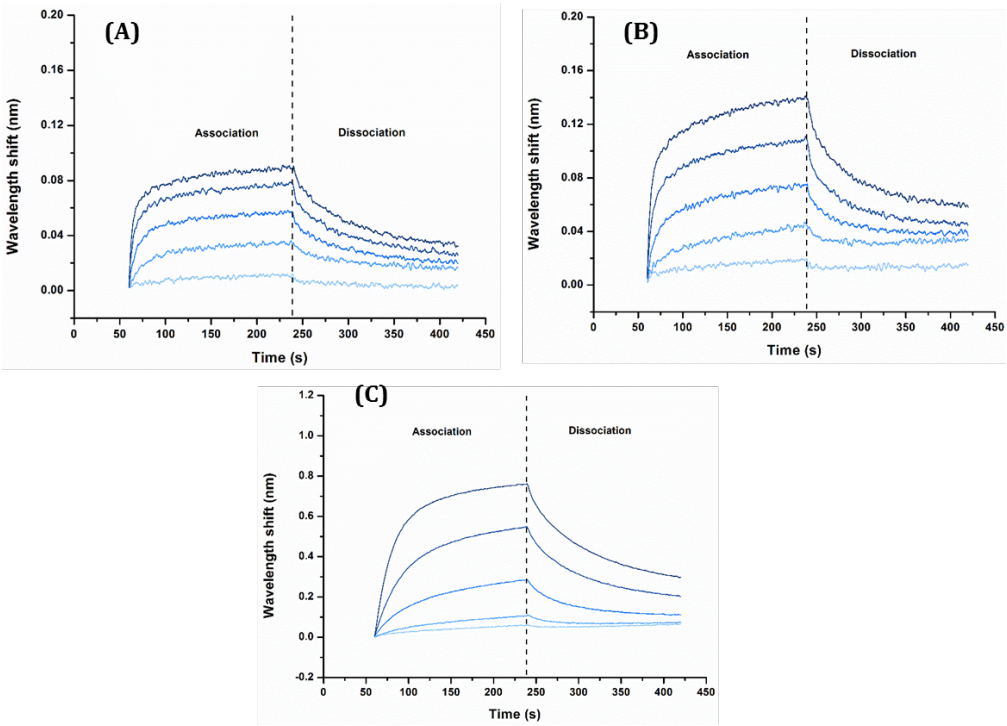

Figure S33: BLI sensorgrams for the interaction of **1a** with G2T1 (A), G1 (B) and HP GC (C). The analyte concentrations were 100; 250; 500; 1000 and 2500 nM in sodium buffer.

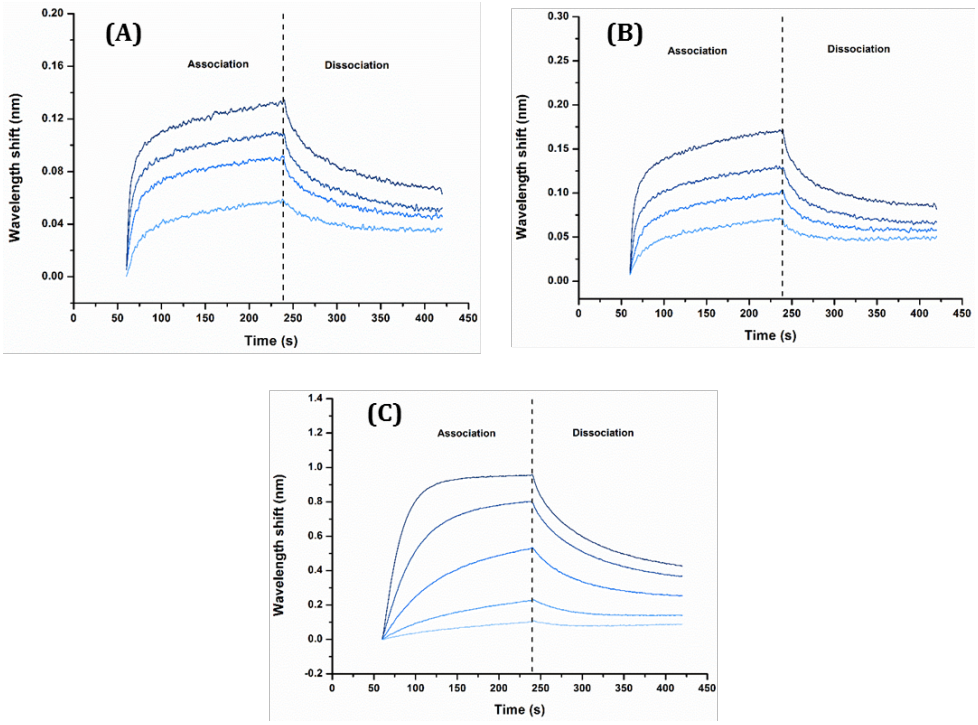

Figure S34: BLI sensorgrams for the interaction of **1b** with G2T1 (A), G1 (B) and HP GC (C). The analyte concentrations were 100; 250; 500; 1000 and 2500 nM in sodium buffer.

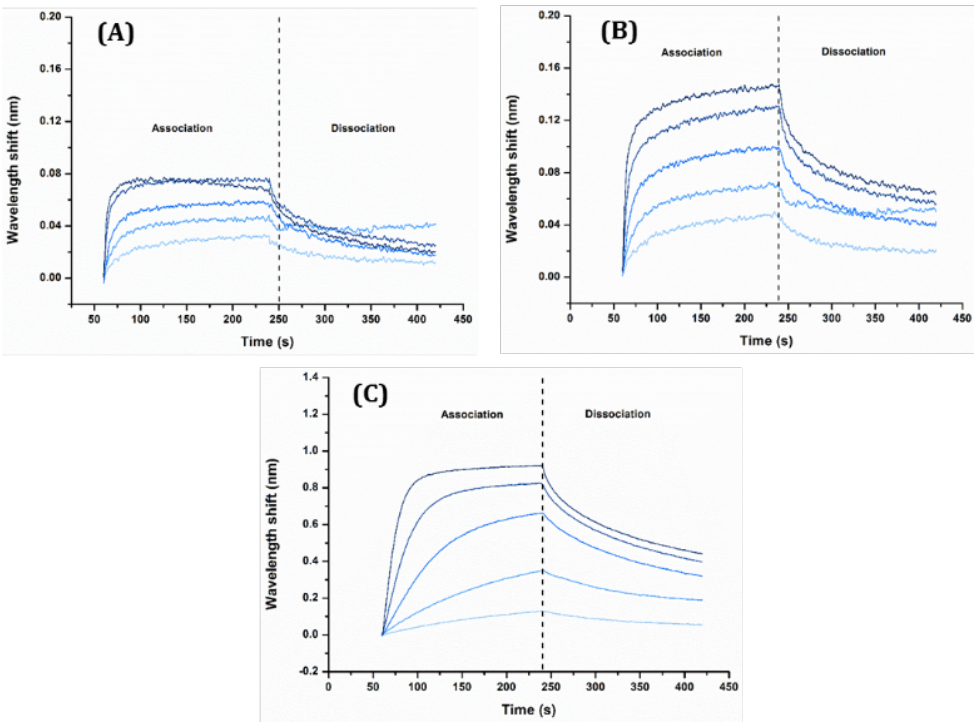

Figure S35: BLI sensorgrams for the interaction of **1c** with G2T1 (A), G1 (B) and HP GC (C). The analyte concentrations were 100; 250; 500; 1000 and 2500 nM in sodium buffer.

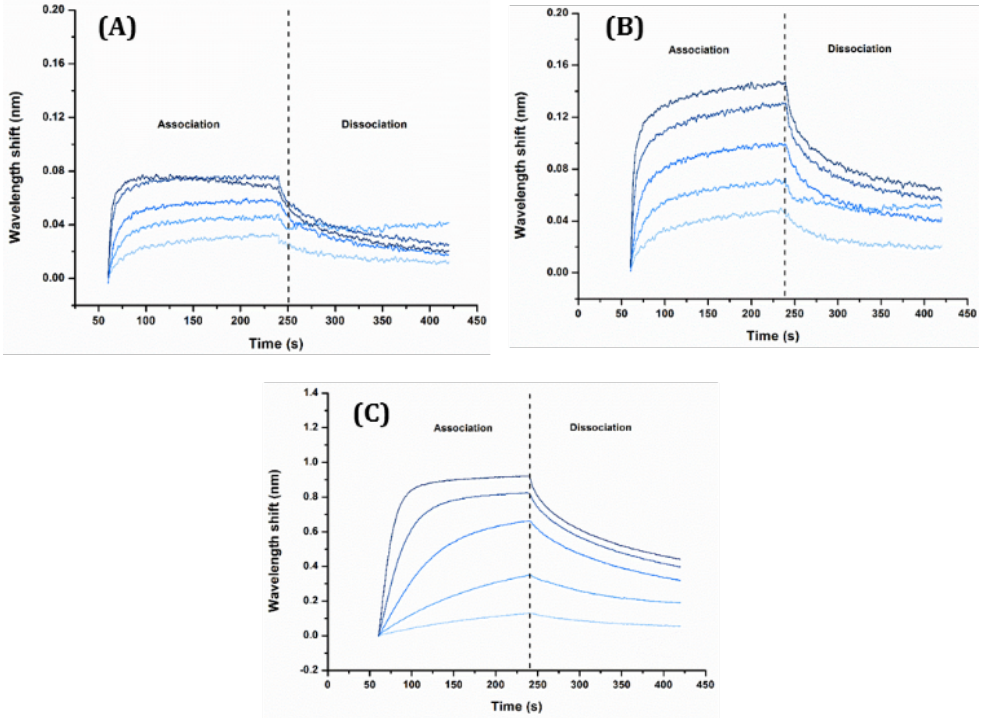

Figure S36: BLI sensorgrams for the interaction of 2a with G2T1 (A), G1 (B) and HP GC (C). The analyte concentrations were 100; 250; 500; 1000 and 2500 nM in sodium buffer.

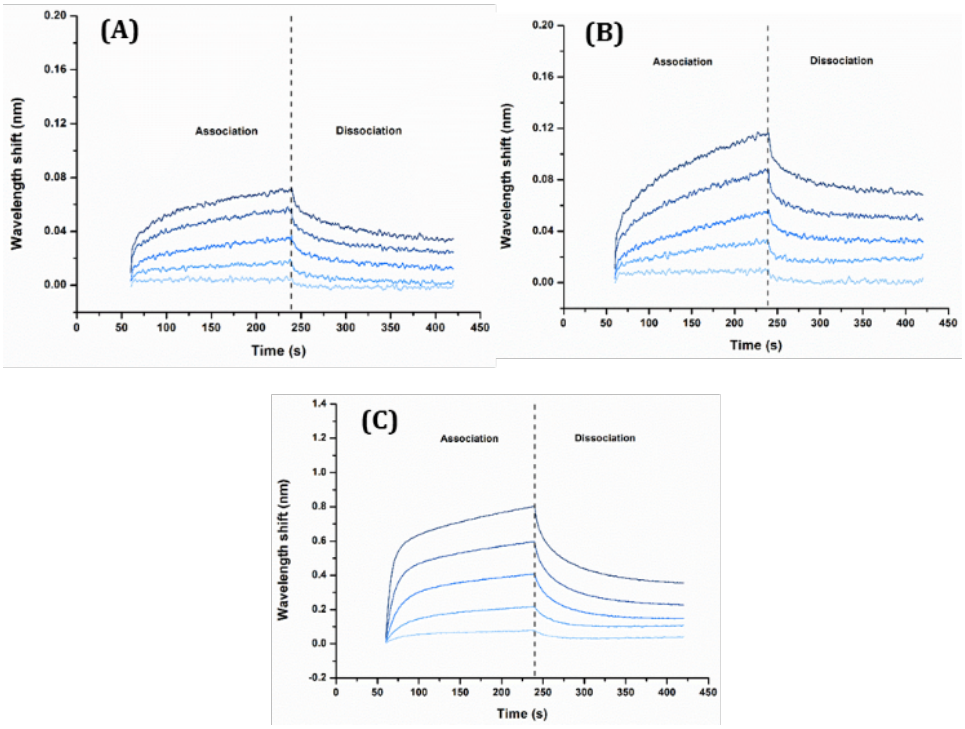

Figure S37: BLI sensorgrams for the interaction of **Ru 2b** with G2T1 (A), G1 (B) and HP GC (C). The analyte concentrations were 100; 250; 500; 1000 and 2500 nM in sodium buffer.

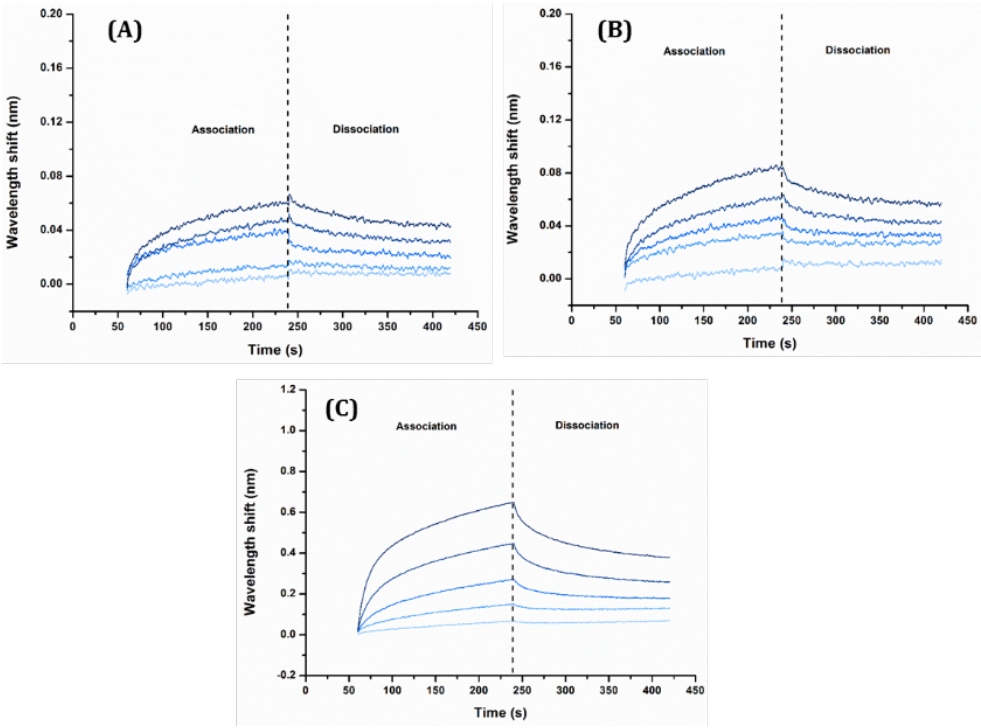

Figure S38: BLI sensorgrams for the interaction of **Ru 2c** with G2T1 (A), G1 (B) and HP GC (C). The analyte concentrations were 100; 250; 500; 1000 and 2500 nM in sodium buffer.

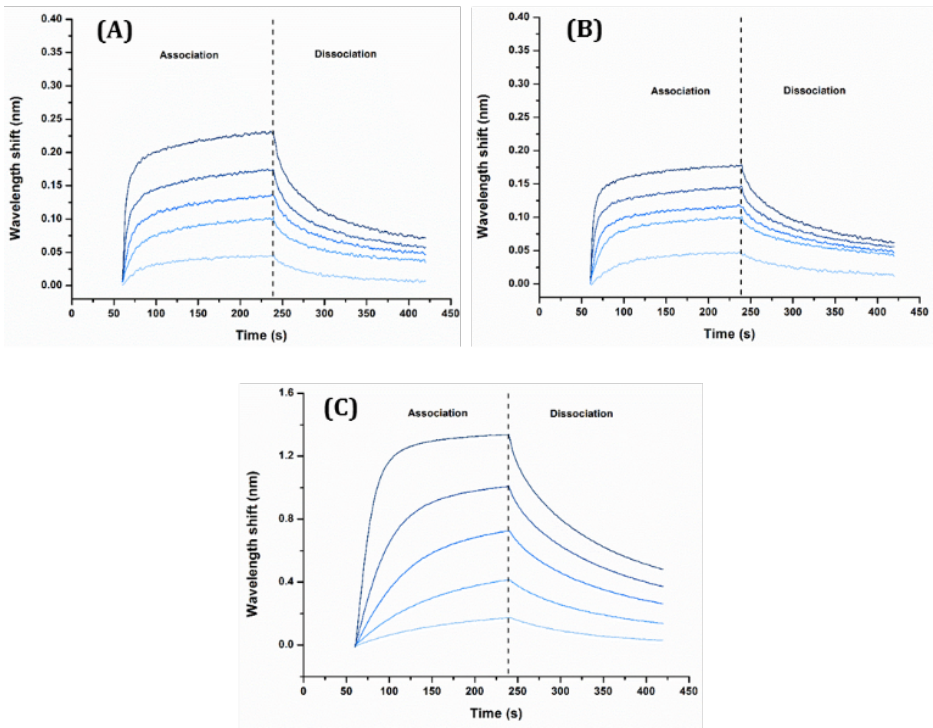

Figure S39: BLI sensorgrams for the interaction of **Ru 1a** with G2T1 (A), G1 (B) and HP GC (C). The analyte concentrations were 100; 250; 500; 1000 and 2500 nM in potassium buffer.

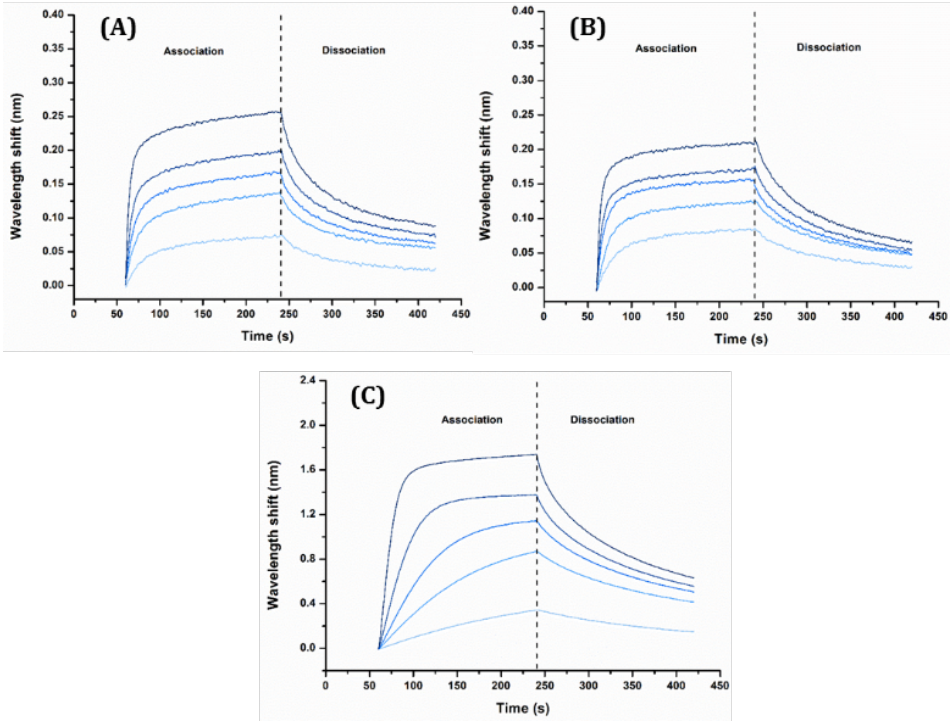

Figure S40: BLI sensorgrams for the interaction of **Ru 1b** with G2T1 (A), G1 (B) and HP GC (C). The analyte concentrations were 100; 250; 500; 1000 and 2500 nM in potassium buffer.

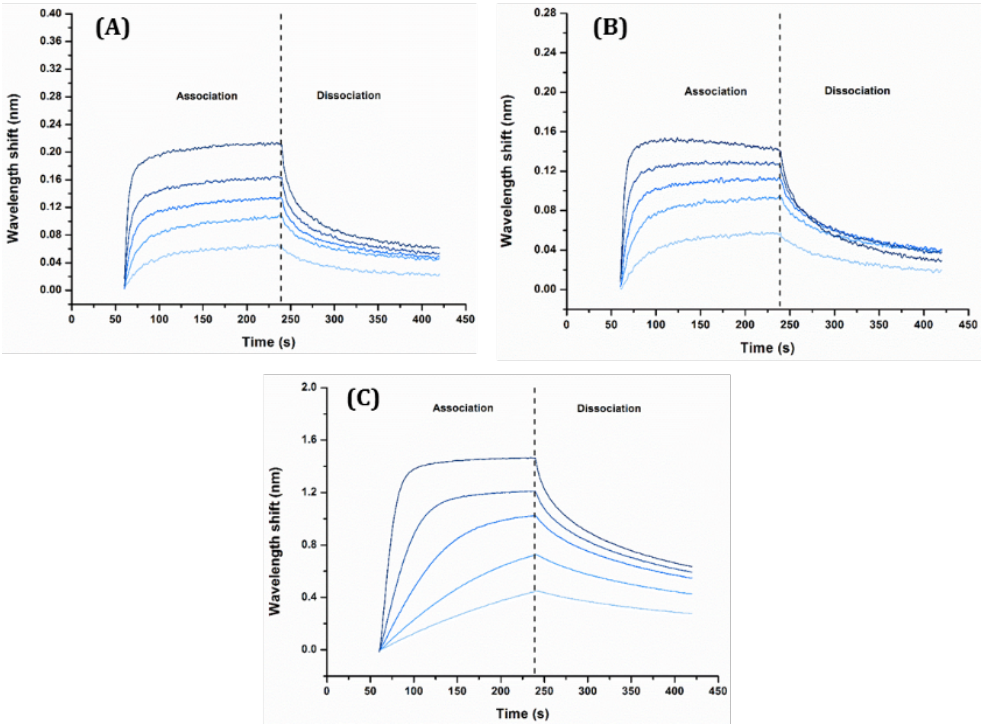

Figure S41: BLI sensorgrams for the interaction of **Ru 1c** with G2T1 (A), G1 (B) and HP GC (C). The analyte concentrations were 100; 250; 500; 1000 and 2500 nM in potassium buffer.

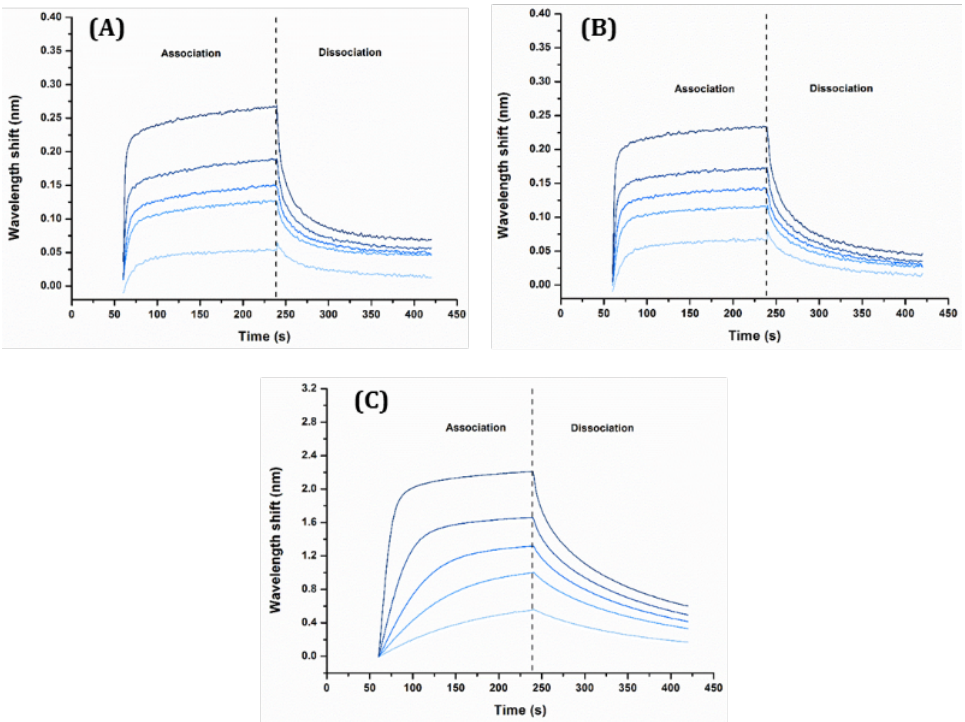

Figure S42: BLI sensorgrams for the interaction of **Ru 2a** with G2T1 (A), G1 (B) and HP GC (C). The analyte concentrations were 100; 250; 500; 1000 and 2500 nM in potassium buffer.

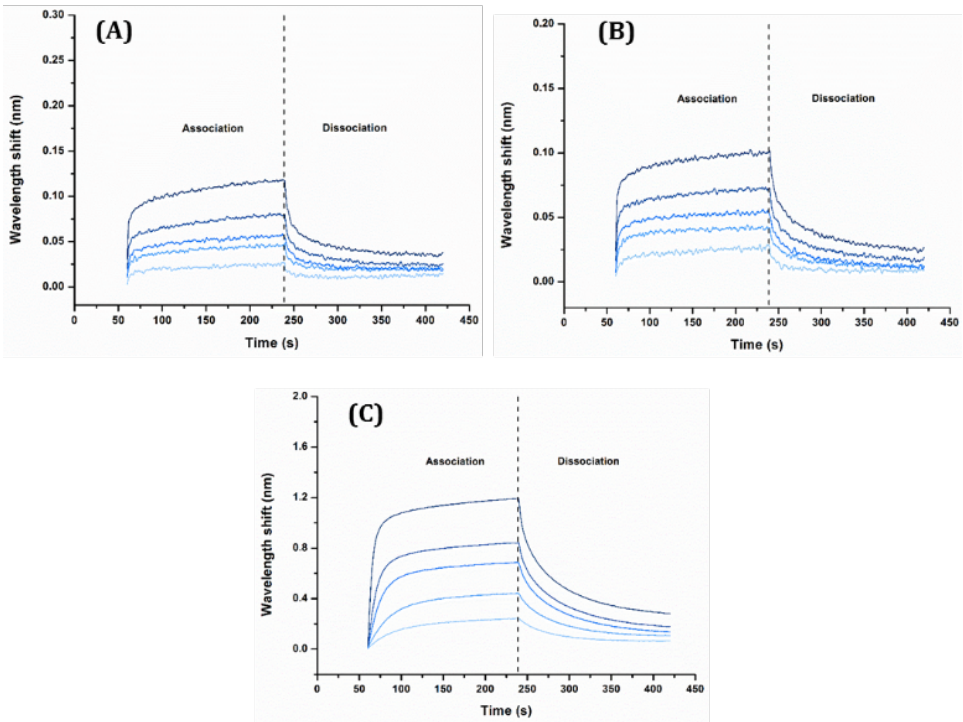

Figure S43: BLI sensorgrams for the interaction of **Ru 2b** with G2T1 (A), G1 (B) and HP GC (C). The analyte concentrations were 100; 250; 500; 1000 and 2500 nM in potassium buffer.

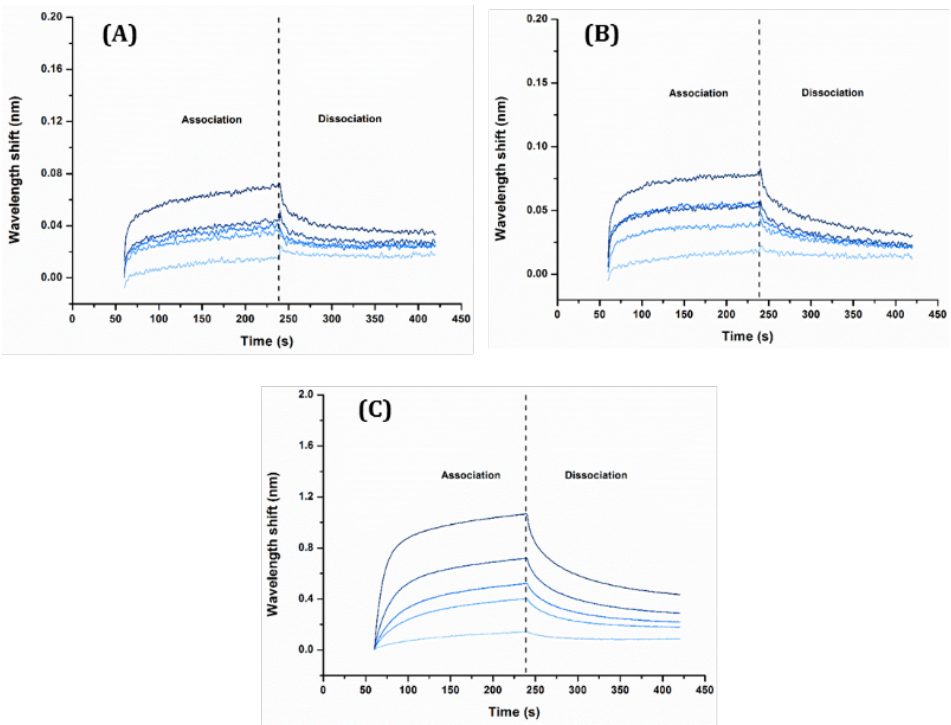

Figure S44: BLI sensorgrams for the interaction of **Ru 2c** with G2T1 (A), G1 (B) and HP GC (C). The analyte concentrations were 100; 250; 500; 1000 and 2500 nM in potassium buffer.

10. Cell penetration experiments

U2OS cells cultures were grown at 37 °C in a humidified atmosphere with 5 % CO_2 in DMEM medium (Westburg) containing 10% foetal bovine serum (FBS) (Gibco) and 1% penicillin/streptomycin (Westburg). 20 000 cells were seeded onto coated microscope slide and incubated with 10 µM of complexes **1a-c** and 50 µM of complexes **2a-c**, for 1h30 in the dark. After incubation, the medium containing the complex was removed, and fresh medium was added to the cells. The cells were rinsed in pre-warmed PBS, fixed in 4 % paraformaldehyde (VWR) for 15 min, labelled with Draq5 (eBioscience) following the instructions of the manufacturer. A confocal laser scanning microscopy system (Zeiss LSM 710) was used to acquire the images. Pictures were processed with Zen software.

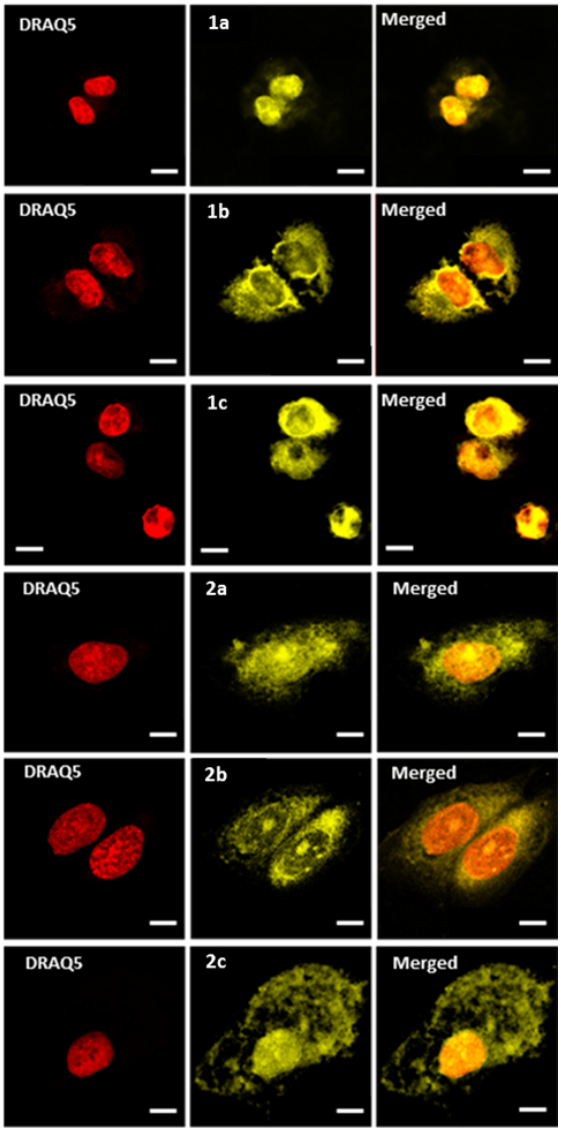

Figure S45: Fluorescence microscopy images of U2OS cells after incubation (1h30) with **1a-c** (10 µM) or **2a-c** (50 µM)* complex in DMEM buffer. From left to right: the nucleus in red, stained by DRAQ5; **1a-c** and **2a-c** complexes in yellow and merged images. Scale, 10 µM.

11. Photo-cytotoxicity experiments

U2OS cells were cultured in 96-well plates for 24h in DMEM (Westburg) containing 10% foetal bovine serum (FBS) (Gibco) and 1% penicillin/streptomycin (Westburg) to reach a density of 12 000 cells/well. The medium was removed and fresh one containing the appropriate concentration of the complexes was added. After 1h of incubation at 37 °C in the dark, cells were rinsed twice with PBS to remove non-internalized complexes. Illumination was performed during 30 minutes with blue LED (LED strip IP68 60 LED/m from Prolumia, 405 nm at 15.7 W/m^2). The distance between the light source and the culture plate was of 10 cm. Before illumination, cultures were rinsed with PBS and illuminated in PBS to avoid absorption by coloured culture medium. Plates serving as a dark control were protected from illumination with aluminium foil. Illuminated and control cultures were put back immediately to the incubator at 37 °C in a humidified environment and cultured in fresh culture medium for an additional 24 h. The cell viability was measured 1 day post-irradiation using 10 µl/well of WST-1 reagent (Sigma-Aldrich) following the manufacturer's instructions. The ratio of the optical density at λ = 450 nm under each set of conditions relative to that of control cells (non-transfected and non-irradiated, 100% viability) was used to determine a relative viability. The measurements were performed twelve times.

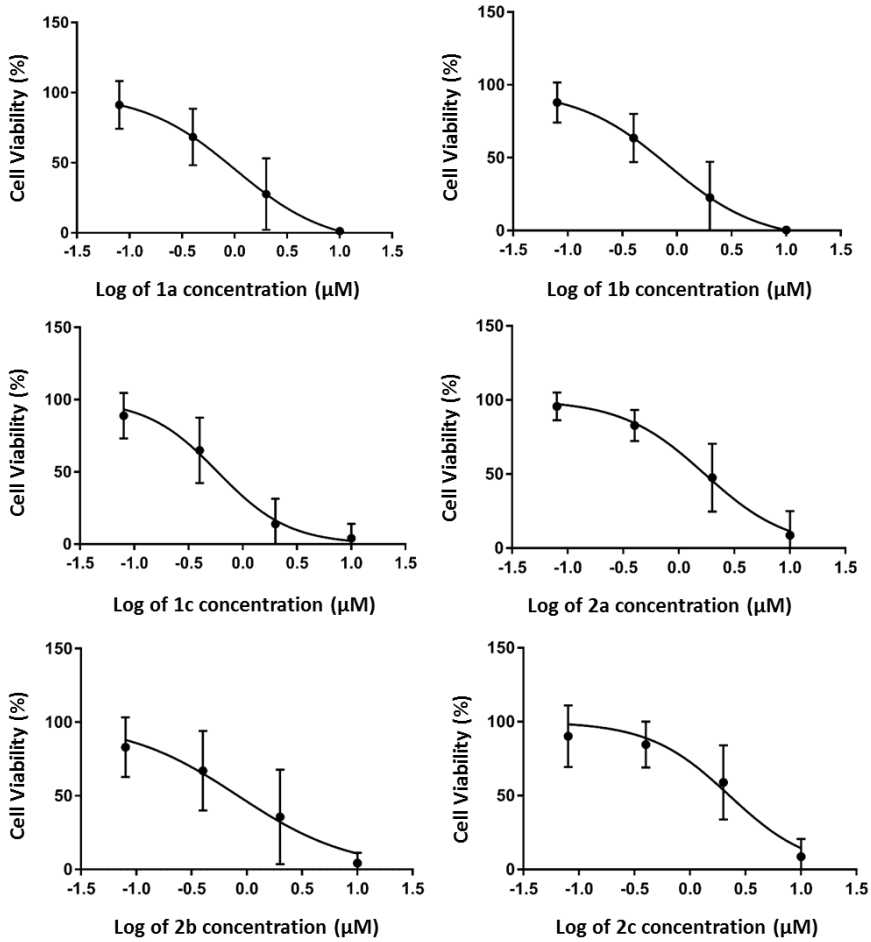

Figure S46: IC_{50} curves of the viability of U2OS cells in the presence of different concentrations of the six complexes under irradiation.

12. Telomere dysfunction-Induced Foci (TIF)

Immunofluorescence was performed as described previously using the anti-53BP1 antibody (#NB100-304) from Novus Biologicals (RRID: AB_10003037).[8] Telomeric sequences were detected via hybridization with a TeloG Exiqon LNATMred probe: (TAMRA) GGGTtAGGGttAGgGTTAGGGttAGGGttAGGGtTA (TAMRA) (small letters indicate LNATM modified bases). Briefly, cells seeded on four-well slides the day before were washed twice with PBS and cytoplasm was pre-extracted with permeabilization buffer (20 mM Tris–HCl pH 8.0, 50 mM NaCl, 3 mM MgCl2, 300 mM sucrose, 0.5% Triton X-100). Once fixed with 3.7% formaldehyde and 2% sucrose in PBS 1× for 15 min at RT, cells were washed with 1× PBS and permeabilized again for 10 min at RT. Following three washes with 1× PBS, cells were blocked for 1 h at 37°C with blocking solution (10% normal goat serum, 1% BSA, 0.1% Triton X-100 in PBS) and subsequently treated with primary antibodies in the Blocking solution overnight at 4°C. The next day, cells were washed three times with PBS-Tween (0.1%) at 45°C and incubated with the secondary antibody for 40 min at 37°C. Cells were washed again three times with PBS-Tween (0.1%) at 45°C followed by three washes with 1× PBS at RT. For POLD3- RAP1 co-staining, both antibodies were added together, overnight in 5% BSA-PBS-Tween (0.1%). The next day, cells were washed three times with PBSTween (0.1%) at RT for 10 min each and incubated with the secondary antibody for 1 h at RT. Subsequently, cells were washed again three times with PBS-Tween (0.1%) and three times with 1× PBS at RT, 10 min and 5 min each, respectively. In the absence of FISH, cells were air-dried and mounted with 20–25 µl/well mounting medium (23.5 mg/ml DABCO (Sigma-Aldrich), 20 mM Tris–HCl pH 7.4, 90% v/v glycerol) containing 0.6 µg/ml DAPI. For telomeric DNA FISH after IF, cells were re-fixed for 2 min with 3.7% formaldehyde in 1× PBS and incubated with 0.1 mg/ml RNAse A for 1 h at RT. Cells were then washed three times with 2× SSC, re-permeabilized for 10 min, briefly washed with 1× PBS, and fixed again with 3.7% formaldehyde. Cells were serially dehydrated, 2 min each, with 70, 80, 90, and 100% ethanol, air-dried, overlaid with 35 ll hybridization solution (160 nM TeloG Exiqon LNATMred probe, 50% deionized formamide, SSC 2×, Blocking reagent 1×), and incubated at 83°C for 3 min with a coverslip. For native FISH, cells were incubated for 1 h with the probe under non-denaturing conditions, at room temperature. Then, unbound probe was washed off successively as follows: 2 × 15 min in 50% formamide, SSC 2×, 20 mM Tris–HCl pH 7.4, and 3 × 5 min in 150 mM NaCl, 0.05% Tween-20, 50 mM Tris–HCl pH 7.4. Slides were serially dehydrated again and mounted with mounting medium containing DAPI as described above. Images were acquired with the Cell Observer Spinning Disk confocal microscope (Zeiss) with 100× objective and analyzed using ImageJ software (National Institute of Health), while maintaining the same threshold for samples from the same experiment. Experiments were repeated at least three times.

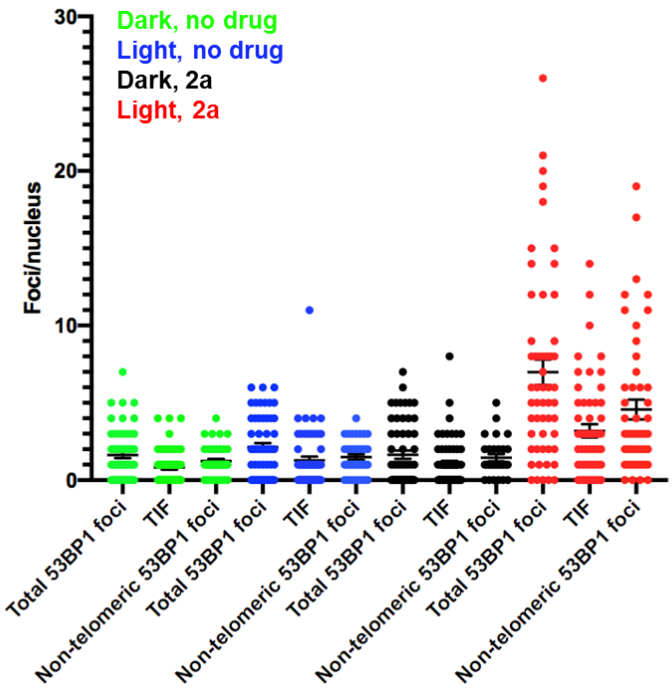

Figure S47: U2OS cells were treated with complex **2a** as indicated in Fig. 3 legend. The total number of 53BP1 foci, the number of TIF and the number of non-telomeric 53BP1 foci are indicated for each nucleus analyzed. Mean ± SEM.

13. Singlet oxygen quantum yield measurements

The singlet oxygen quantum yields of compounds **1a** and **2a** (phen and TAP analogs) were determined in water by monitoring the decomposition of a $^1O_2$ trap (AVS = Anthracene-9,10-diVinylSulfonate) on a time range extending from 0 to 15 minutes. Practically, an aerated solution containing AVS (Absorbance ≈ 1 at 405 nm) and the photosensitizers (Absorbance ≈ 0.050 at 465 nm) was irradiated at 465 nm using a light source from a spectrofluorometer (8 V 450 W Xenon Short Arc lamp). The decomposition of AVS was then determined by analyzing the absorption decay of AVS at 395 nm.

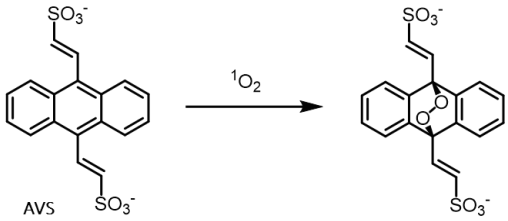

Figure S48: Reaction of AVS with singlet oxygen.

The singlet oxygen quantum yields were calculated by a relative method using fluorescein (Φ_Δ = 0.03) as the reference.

$$\Phi_\Delta(Ru) = \Phi_\Delta(ref) * \frac{Abs_{465nm}(ref)}{Abs_{465nm}(Ru)} * \frac{k(Ru)}{k(ref)}$$

k(Ru) and k(ref) are the slope of plots of the AVS absorption decay (at 395 nm) associated to the photo-oxidation induced by compounds **1a and 2a** and the reference compound fluorescein.

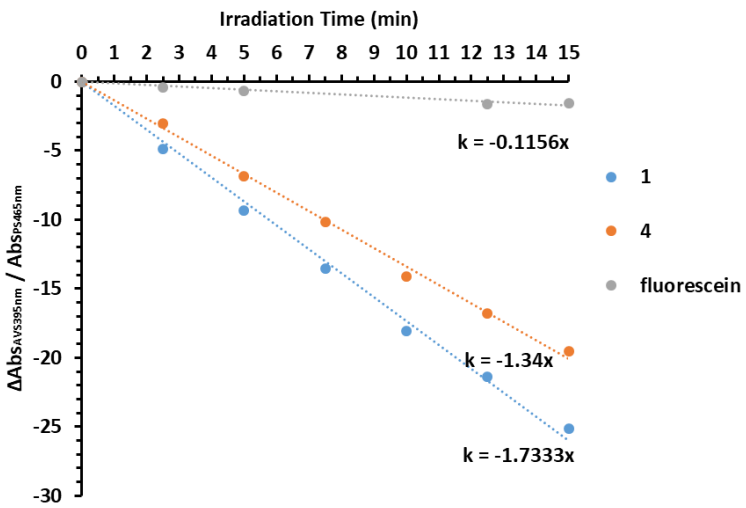

Figure S49: AVS decomposition monitoring using compounds **1, 4 and fluorescein** as photosensitizers.

Compound	1a	2a	Fluorescein
Φ_Δ	0.41	0.32	0.03

13. References

(1) Ju, C.-C.; Zhang, A.-G.; Yuan, C.-L.; Zhao, X.-L.; Wang, K.-Z., The interesting DNA-binding properties of three novel dinuclear Ru(II) complexes with varied lengths of flexible bridges. *Journal of Inorganic Biochemistry* **2011**, *105* (3), 435-443.

(2) Jacquet, L.; Mesmaeker, A. K.-D., Spectroelectrochemical characteristics and photophysics of a series of RuII complexes with 1,4,5,8,9,12-hexaazatriphenylene: effects of polycomplexation. *Journal of the Chemical Society, Faraday Transactions* **1992**, *88* (17), 2471-2480.

(3) Masschelein, A.; Jacquet, L.; Kirsch-De Mesmaeker, A.; Nasielski, J., Ruthenium complexes with 1,4,5,8-tetraazaphenanthrene. Unusual photophysical behavior of the tris-homoleptic compound. *Inorganic Chemistry* **1990**, *29* (4), 855-860.

(4) Liu, Y.; Duan, Z.-Y.; Zhang, H.-Y.; Jiang, X.-L.; Han, J.-R., Selective Binding and Inverse Fluorescent Behavior of Magnesium Ion by Podand Possessing Plural Imidazo[4,5-f]-1,10-phenanthroline Groups and Its Ru(II) Complex. *The Journal of Organic Chemistry* **2005**, *70* (4), 1450-1455.

(5) Brouwer Albert, M., Standards for photoluminescence quantum yield measurements in solution (IUPAC Technical Report). *In Pure and Applied Chemistry* **2011**, *83*, 2213.

(6) Boros, J.; Arnoult, N.; Stroobant, V.; Collet, J.-F.; Decottignies, A., Polycomb repressive complex 2 and H3K27me3 cooperate with H3K9 methylation to maintain heterochromatin protein 1α at chromatin. *Mol Cell Biol* **2014**, *34* (19), 3662-3674.

(7) Diman, A.; Boros, J.; Poulain, F.; Rodriguez, J.; Purnelle, M.; Episkopou, H.; Bertrand, L.; Francaux, M.; Deldicque, L.; Decottignies, A., Nuclear respiratory factor 1 and endurance exercise promote human telomere transcription. *Science Advances* **2016**, *2* (7), e1600031.

(8) Episkopou, H.; Diman, A.; Claude, E.; Viceconte, N.; Decottignies, A., TSPYL5 Depletion Induces Specific Death of ALT Cells through USP7-Dependent Proteasomal Degradation of POT1. *Mol. Cell* **2019,** *75* (3), 469-482.e6.